JOURNAL OF MATERIALS SCIENCE **39** (2004) 6757–6779

The use of neutron scattering in the study of ceramics

S. M. BENNINGTON
ISIS Pulsed Neutron Source, Rutherford Appleton Laboratory, Chilton, Didcot, Oxfordshire, OX11 0QQ, UK
E-mail: s.m.bennington@rl.ac.uk

Neutron scattering is a versatile probe used to study the structure and dynamics of materials. It has particular relevance to the investigation of ceramics and has been used in their study since neutron scattering was first developed almost sixty years ago. This review will focus on the relative merits of neutron scattering compared to other microscopic probes, with particular reference to ceramic materials, and will illustrate the uses of neutron diffraction and inelastic neutron scattering in various key fields of ceramic research.

1. Introduction

Neutron scattering techniques, in particular neutron diffraction, have been used to study ceramics almost from the birth of neutron scattering in the 1940's, and provides microscopic information on the atomic structure and dynamics of materials [1, 2]. As well as advancing our fundamental understanding of condensed matter, neutron scattering has made important contributions to a wide range of technologically important materials, ranging form bio-polymers to exotic superconductors.

With today's large central facilities, such as the Institute Laue Langevin in France and ISIS in the UK, neutron scattering is an established and widely accessible technique. Its usefulness and versatility has been widely recognised and investment is being made available for more advanced sources, including upgrades at ISIS (such as the construction of a second target station), and powerful new spallation neutron sources in the USA and Japan as well as new reactors at Munich in Germany and Lucas Heights in Australia.

In the field of ceramics the use of neutrons has traditionally been dominated by diffraction, and although still the most important, other techniques are increasingly being used. Small angle scattering and surface reflection are valuable for certain problems, particularly in complex systems with multiple phases or interfaces, and spectroscopic measurements supply unique information which is a natural partner to the powerful ab-initio computer simulation codes that have been developed over the last decade.

A comprehensive overview of the use of neutron scattering in the study of ceramics is probably not possible in a review of this kind, and this article makes no pretence to be complete. Its aim, is to discuss the relative strengths and weakness of the technique compared to other microscopic probes, and then illustrate these points with case studies chosen, partly due to the authors prejudice, and partly because they are of current interest.

2. The properties of the neutron

2.1. The properties of the neutron

The usefulness of the neutron stems from its physical properties namely: its lack of charge, its magnetic moment and its mass. Because it has no charge, the neutron does not interact with electrons in the way that electromagnetic radiation does; instead it interacts with the nucleus, via the nuclear strong force. The mass of a neutron is similar to the mass of atomic nuclei, which means that both its momentum and energy are similar to those of atoms in normal matter. Specifically this means that it is possible to use neutrons to study both the structure and dynamics of a material, in some cases simultaneously. This is not the case with electromagnetic probes; X-rays have wavelengths of the order of interatomic spacings, but their energies are many orders magnitude greater then those in condensed matter, and optical radiation has energies similar those of excitations in matter but has wavelengths of several thousands of Angstroms.

2.2. The interaction of neutrons with matter

Neutrons interact in one of three ways:

(1) By scattering from the nucleus of the atom
(2) By being absorbed by the nucleus of the atom
(3) Through the magnetic moments of the electrons

In the vast majority of neutron scattering experiments information is extracted from the direction and wavelength of the scattered neutrons rather than from those lost to absorption. And like many other scattering techniques most of the structural information is taken from the interference patterns of these scattered neutrons.

Diffraction patterns are related to the Fourier Transform of the real space structure. Because X-rays interact with the electronic charge distribution of an atom (with a length scale of around 10^{-10} m) the amplitude of an X-ray diffraction pattern drops away rapidly with scattering vector with an envelope (or form factor) which is related to the inverse of the size and distribution of the charge. Neutrons, by contrast, interact with the nucleus of an atom, whose typical dimension is five orders of magnitude smaller than the neutrons wavelength (10^{-15} m compared to 10^{-10} m). As far as the neutron is concerned the scattering potential has no dimension and so a neutron diffraction pattern does not die away with scattering vector, it has no form factor. This means that neutron diffraction is particularly useful in determining complex structures or observing subtle structural changes as a function of an external parameter, such as temperature, pressure or composition. Unlike nuclear scattering, the neutrons magnetic interaction is via the atoms unpaired electrons and so magnetic scattering has a form factor similar to that for X-ray scattering.

There are also various techniques that use neutron absorption in elemental analysis. The gamma rays produced from the excited nucleus are characteristic of the element and isotope and can be used to map the spatial distribution of a neutron absorbing element in a sample, in a completely non-destructive way.

2.3. The variation of cross-section with atomic number

The strength of the interaction of a neutron with an atom is defined in terms of a cross-section with symbol σ and has units of area. By convention the cross-section is defined in terms of a scattering-length, symbol b, by:

$$\sigma = 4\pi b^2 \tag{1}$$

Although the magnetic and nuclear interactions have completely different physical origins, their cross-sections are conveniently similar. The fact that many of first successes of the early pioneers of neutron scattering were in the understanding of magnetic structures and the fact that the neutron continues to be the probe of choice for magnetic studies today, is due to this fortuitous coincidence.

Neutron scattering cross-sections do not vary systematically with atomic number. The variation of the total scattering lengths can be seen in Fig. 1. Neighbouring atoms in the periodic table can have wildly different cross-sections, making it possible to get contrast that would not be visible with other techniques. For example ions with similar or equal numbers of electrons such as Ti^{4+}, Ca^{2+} and K^{+}; or K^{+} and Cl^{-}; or Na^{+}, Mg^{2+}, Al^{3+} and Si^{4+}; or Fe^{2+} and Mn^{2+}, all have very similar cross-sections for X-ray scattering, but significantly different scattering lengths for neutron diffraction. Understanding the ordering of these cations by X-rays can only be done indirectly by careful analysis of bond lengths, a technique that is unfortunately prone to errors as bond lengths are also affected by factors such as site-occupancy. Neutron scattering can be used to directly and systematically study cation ordering and site-occupancy.

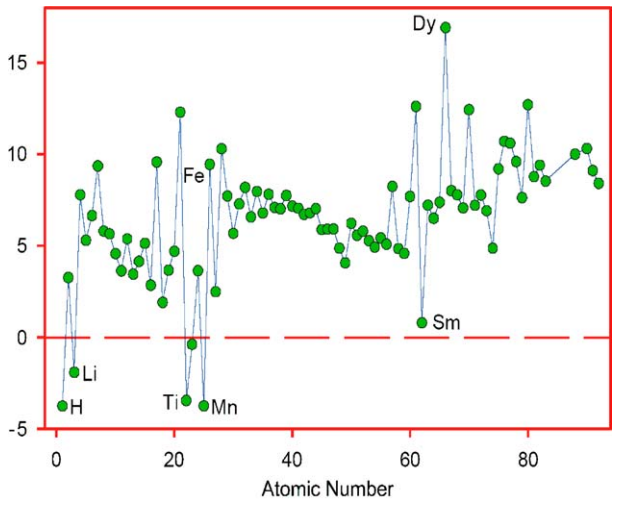

Figure 1 The dependence of the total neutron scattering lengths as a function of atomic number.

Because X-ray scattering cross-section is directly related to the number of electrons light atoms such as hydrogen, lithium or oxygen are often very difficult to locate in the presence of heavier elements. Although they vary from element to element, the neutron cross-sections do not vary so much and light elements often have cross-section greater then those higher in the table. For studies such as oxygen disorder or lithium diffusion neutron scattering is an ideal probe.

2.4. Coherent and incoherent scattering

When calculating the scattering from a material we generally average over all the elements in a material. However, the scattering length for an element is dependent on its isotope and nuclear spin state. For many important elements this is not an issue. For example oxygen has three common isotopes ^{15}O, ^{16}O and ^{17}O, which occur with relative abundances of 1, 98 and 1% respectively; justifying an assumption of a constant scattering length. However, there are significant exceptions. The two isotopes of nickel are ^{58}Ni (68% abundance) and ^{60}Ni (26.1%) with cross-sections of 14.4 and 2.8 fm with neither isotope having a non-zero nuclear spin. This means that for a significant fraction of the scattering there is no correlation between the phases of the scattered neutrons. This is known as *incoherent* scattering and does not produce a diffraction pattern.

If f_i is the relative frequency that the cross-section b_i occurs then the average value of b is

$$\bar{b} = \sum_i f_i b_i \tag{2}$$

and the average value of b^2 is

$$\overline{b^2} = \sum_i f_i b_i^2 \tag{3}$$

The cross-sections are defined as

$$\sigma_{coh} = 4\pi(\bar{b})^2 \quad \text{and} \quad \sigma_{inc} = 4\pi\{\overline{b^2} - (\bar{b})^2\} \tag{4}$$

Coherent scattering depends on the correlation between the positions of the same type of nucleus and contains interference information, whereas incoherent

scattering, depends on the cross-section of single atoms and contains no interference effects. A tabulation of neutron cross-sections can be found in the report by Sears [3].

One element in particular stands out as unique in neutron scattering. Hydrogen (^{1}H) has the largest total cross-section of any element in the periodic table. Almost all of this is incoherent, but it not due to isotopic randomness but due to the spin of the nucleus. The proton and the neutron both have a spin of 1/2, which when combined have a total spin of either $S = 1$ when aligned parallel, and $S = 0$ when antiparallel. The scattering lengths for the parallel arrangement is 10.4 fm and for the antiparallel is -47.4 fm, but because there are three possible parallel arrangements ($S_z = -1, 0$ and $+1$) the average is only -3.74 fm. Thus hydrogen has a very small coherent, but a large incoherent cross-section. The hydrogen cross-section is in fact almost an order of magnitude larger than that of any other element, and so it will dominate the scattering from any material that contains it. This will tend to mask the Bragg scattering and make structural analysis problematic. However, the cross-section from deuterium is entirely coherent; thus replacing hydrogen with deuterium is a powerful technique in neutron scattering and we will see examples of this later. The large cross-section for hydrogen also has advantages particularly in spectroscopy in cases where it is the dynamics of the hydrogen that are of interest.

2.5. The scattering function

A typical scattering experiment will involve measuring the intensity of the neutrons scattered from a beam incident on a sample. The scattering process will involve a change in the direction and velocity of the neutron as it transfers momentum, and perhaps also energy, to the sample. The momentum transfer ($\hbar\boldsymbol{Q}$) is proportional to the scattering vector $\boldsymbol{Q}$, and the energy transfer is related to some dynamic fluctuation in the sample by $E = \hbar\omega$. The intensity measured in an experiment is converted into a function of $\boldsymbol{Q}$ and ω known as the dynamic scattering function, $S(\boldsymbol{Q}, \omega)$. This function is the Fourier Transform of the time and spatial fluctuations of the atomic density (or spin density for magnetic materials). The attraction of this function is that it contains no neutron related information and is directly accessible through computer modelling or analytical calculation.

This is often separated into coherent and incoherent parts

$$S(\boldsymbol{Q}, \omega) = S_{\text{inc}}(\boldsymbol{Q}, \omega) + S_{\text{coh}}(\boldsymbol{Q}, \omega) \tag{5}$$

It can also be separated into elastic and inelastic scattering. The elastic component occurs at $\omega = 0$ and comes from the time independent part of the scattering system. The small fraction that come from the fluctuations in the system is know as the inelastic scattering

$$S(Q, \omega) = S_{\text{inel}}(Q, \omega) + S_{\text{el}}(Q) \tag{6}$$

Both these terms can be separated into incoherent and coherent parts. Integrating over all energies produces $S(\boldsymbol{Q})$, which is what is measured in a typical diffraction experiment.

2.6. The benefits of weak interaction

In contrast to X-rays or electrons the interaction of neutrons with matter is relatively weak. Whereas the scattering from X-rays is often limited to a few microns of the surface of a material and electrons to a few atomic layers, neutrons are a penetrating probe and can travel many centimetres in most materials. This has various advantages:

(1) Neutrons take a true average of the whole sample. This often means that the information gained from X-rays, electrons and neutrons are different, making them complementary techniques.

(2) Since the probe does not disturb the system it makes it easy to model the results. Neutron scattering is quantitative in a way that few other scattering probes can match. It makes it the natural ally of computational techniques.

(3) This weakness of interaction has other benefits: the radiation does not damage the sample under study, there is no appreciable heat-load and the sample does not require invasive and damaging pre-treatment. It is a truly a non-destructive probe and as such it is increasingly finding application in areas such archaeology or art history where the samples are highly valuable or delicate, or in engineering where whole components can studied in the form they will ultimately be used.

(4) Neutrons have little difficulty in passing through the walls of sample environment equipment, making the use of cryostats and furnaces routine. Although high pressure studies have in the past been the preserve of X-ray scattering, where the small beam sizes and high intensities are highly advantageous; improvement in the power of neutron sources and greater investment in instrumentation mean that neutron diffraction measurements at pressures up to 25 GPa are relatively common [4], with the record currently standing at 47 GPa.

Improvements in source power and neutron instrumentation have permitted an increase the complexity of experiments, and the measurement of real systems under more realistic conditions has become an important theme in modern neutron scattering. For example, it is no longer necessary to infer the operation of complex materials from indirect experiments on model materials. Microscopic studies of: battery or fuel cell materials in operation, the reaction of chemicals in

TABLE I The distance penetrated into various materials (mm) by Cu K_α X-rays until the beam intensity drops to 10% of the initial flux

	Neutrons	X-rays
Be	24.9	9.372
C	37.3	1.886
Al	220.4	0.175
Fe	19.1	0.009
Cd	0.2	0.011
Pb	61.9	0.008

hydrothermal cells or on catalytic surfaces, studies of the structural changes of ferroelectric materials in an electric field or the micro-strain in engineering components under stress, often provides definitive and unambiguous information about the atomic scale behaviour of matter.

3. The sources

The neutron was discovered by Chadwick in 1932 at the Cavendish Laboratory in Cambridge and it did not take very long to realise how important this new particle was going to be. Conventionally neutrons are produced in reactors as the by-product of nuclear fission. And as such neutron scattering has piggy-backed on the development of nuclear reactor design. The first real reactor was the Clinton Pile; a 3 MW graphite reactor built in 1943 in what is now the Oak Ridge National Laboratory in Tennessee, USA. By as early as 1945 it was already being used for neutron scattering measurements. Over the following three decades reactor design improved, arguably reaching a peak in the world's most powerful neutron source at the at the Institute Laue Langevin (ILL) in Grenoble, which first went critical in 1971. The 1980's saw the development of accelerator based neutron sources, including the ISIS pulse neutron source at the Rutherford Appleton Laboratory in Oxfordshire which saw first neutrons in 1984. Although it is currently the world's most powerful pulsed neutron source, new pulsed sources are under construction in USA and Japan which will surpass it in power sometime around 2010.

3.1. The Institute Laue Langevin (ILL)

The ILL is a European funded facility sited in Grenoble in southern France [5]. It is the world's most intense source of neutrons with a wide range of state-of-the-art neutron instrumentation that spans all the possible neutron techniques.

The source is a 58 MW nuclear reactor with a compact, high enriched uranium core cooled with heavy water. The neutrons are produced by nuclear fission at energies around 2–3 Mega-electron volts. These are then allowed to come to thermal equilibrium in moderators to produce neutrons with energies in the milli-electron volt range where their wavelengths are long enough to be useful for diffraction. Several different moderators are used from graphite at 2400 K to liquid deuterium at 25 K to produce neutrons with a range of different wavelengths. Fission reactions work most efficiently with slow neutrons and so all the neutrons that are produced at a reactor are thermalised; as a consequences their flux of high energy, very short wavelength neutrons is comparatively low.

3.2. The ISIS pulsed neutron source

The world's most powerful source of pulsed neutrons is the ISIS spallation source at the Rutherford Appleton Laboratory in Oxfordshire in the UK [6]. This uses a synchrotron to accelerate protons to 800 Mega-electron volts, which are then allowed to interact with a small heavy metal target where neutrons are produced through a spallation reaction. These high energy neutrons are slowed to thermal energies in a series of moderators ranging from water at 300 K to liquid

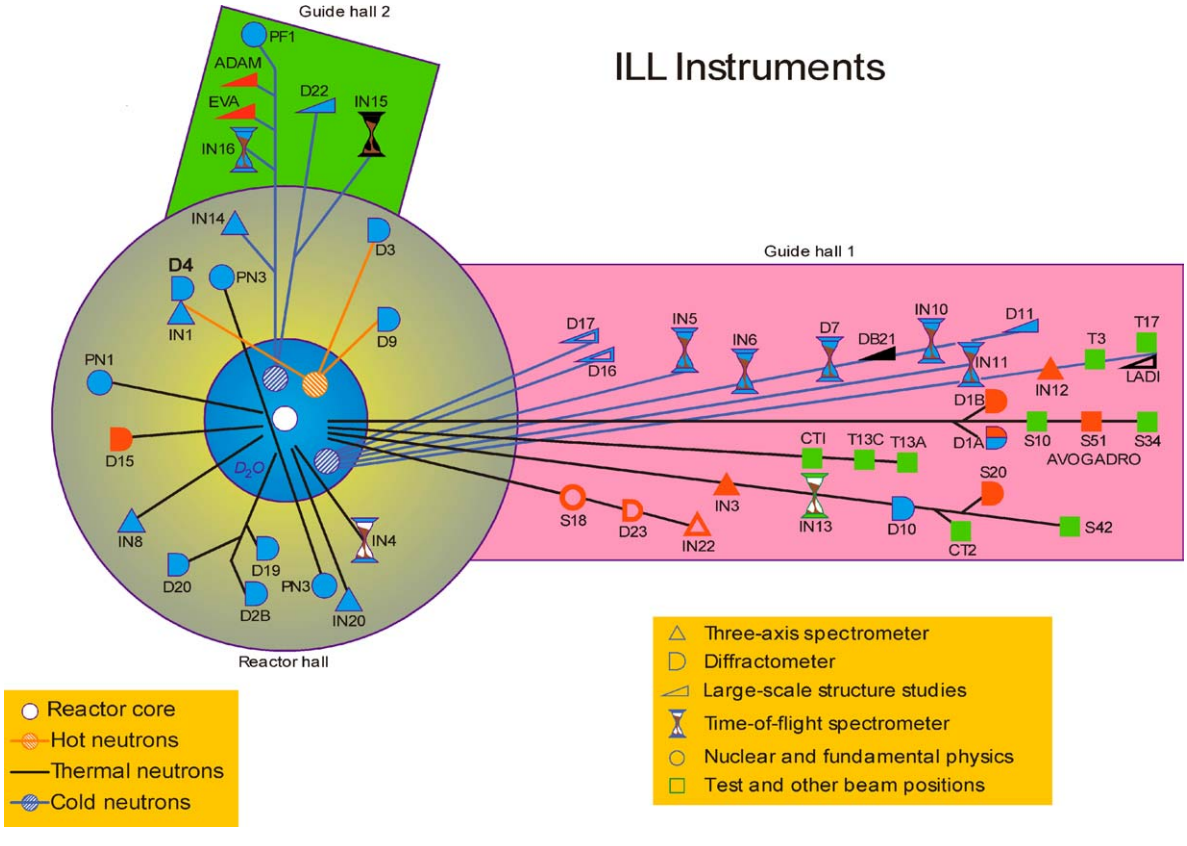

Figure 2 A schematic of the instrument layout around the ILL reactor [5].

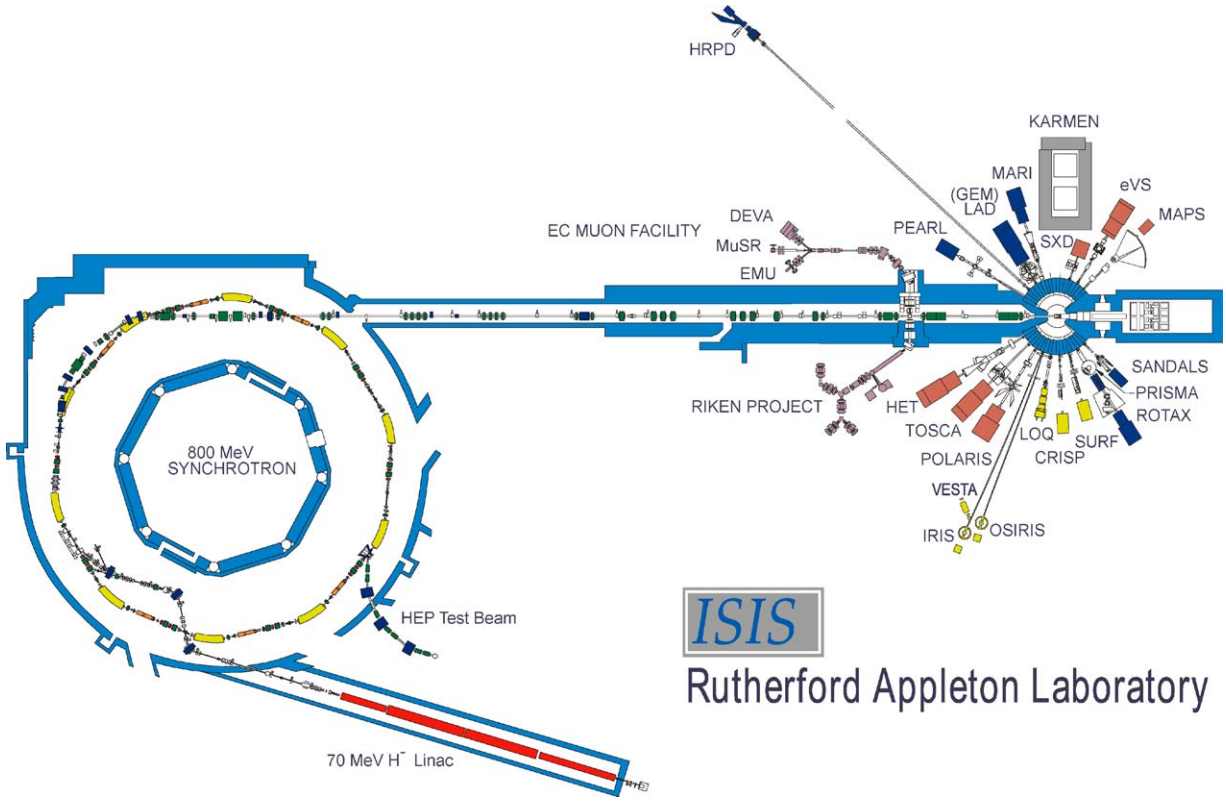

Figure 3 A schematic of the instrument layout around the ISIS target. The second target station is currently under construction and is due for completion in 2007 [6].

hydrogen at 20 K. Because the moderation process plays no part in the production of the neutrons, the moderators are deliberately designed to under-moderate the neutrons, partly to keep the pulse width narrow but also to retain a flux of high energy (∼1 eV) neutrons.

Whereas a nuclear reactor produces neutrons continuously, a pulsed source produces neutrons only when the proton beam hits the target, which at ISIS occurs 50 times per second. At a nuclear reactor a wavelength of neutrons is typically selected by using Bragg scattering from a crystal, but at a pulsed source it more natural to find the speed and hence the wavelength of the neutrons using time-of-flight. Thus the operation and capabilities of the instruments at the two types of source are different and often lend themselves to different kinds of measurements. This level of subtlety is beyond the scope of this article, but of course the instrument scientists at the respective sources are usually more than happy to point out the benefits of their own instruments.

4. The techniques

4.1. Diffraction

The first demonstrations of neutron diffraction were in 1936; only four years after Chadwick first discovered the neutron. But a usable neutron diffractometer had to wait until the discovery of nuclear fission in the early war years and the construction the Clinton Pile reactor at Oak Ridge in 1943. The first diffraction instrument was a crude two-axis machine built in 1945 by Ernest Wollan [7]. Over the next ten years he and Clifford Shull developed the instrumentation and the technique [8], created a library of scattering lengths [9] and performed many classic experiments such as determining the structure of ice [10] and other hydrogen containing systems [11], and providing the first direct evidence for antiferromagnetism [12]. They also developed polarised neutron scattering [13] and were able to separate magnetic and nuclear scattering in ferromagnetic materials [14]. Clifford Shull received a Nobel Prize for this work in 1994. Ernest Wollan only failed to receive the same honour because of his death in 1984.

4.1.1. Instruments for neutron powder diffraction

Because a reactor is a steady state source, it is not possible to use all the wavelengths produced in the moderator simultaneously. To create a diffractometer a single neutron wavelength must be selected by using Bragg reflection from a crystal. This monochromatic beam is then scattered from the sample and a diffraction pattern measured as a function of scattering angle, a technique that will be familiar to anyone who has used a laboratory X-ray source. A modern diffraction instrument (D20) can be seen in Fig. 4 [15]. It has multiple monochromating crystals to give a range of different incident wavelengths and uses position sensitive detectors spanning a 160° angular range to speed up data collection. D20 is a high intensity powder diffractometer able to measure a diffraction pattern over a wide *d*-spacing range in a matter of seconds.

At a pulsed source the wavelength of the neutrons is determined by timing their flight over the length of the spectrometer. Because all the neutrons are produced in a single pulse, by the time they reach the sample they have sorted themselves out in time with the shortest wavelengths arriving first. Thus time of flight diffraction is

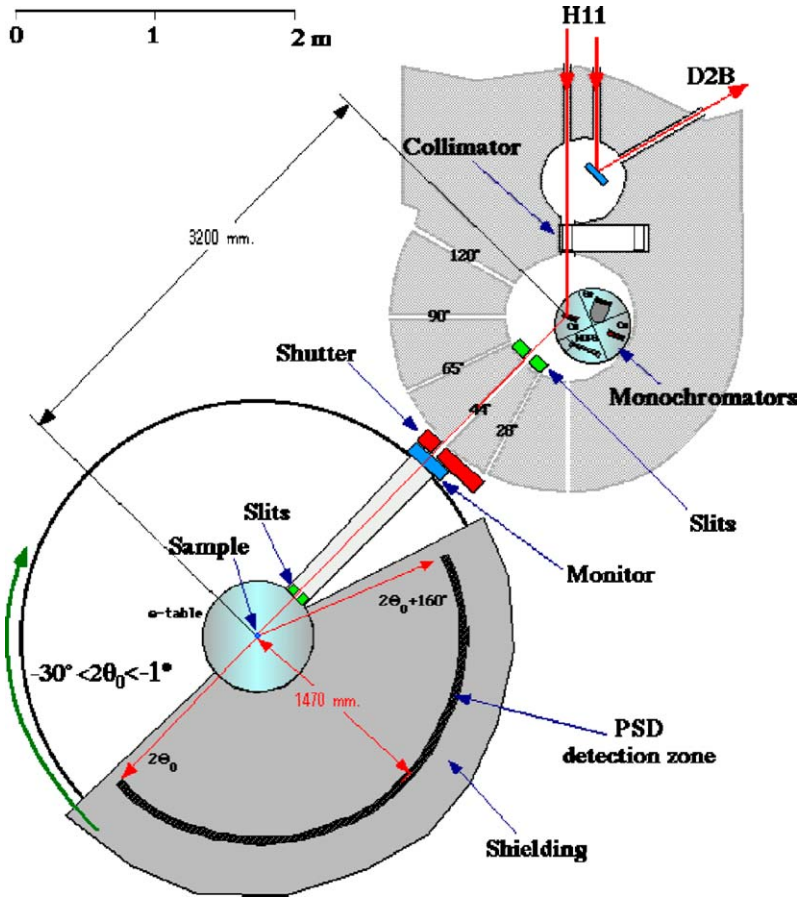

Figure 4 The D20 powder diffractometer at the ILL in France [15].

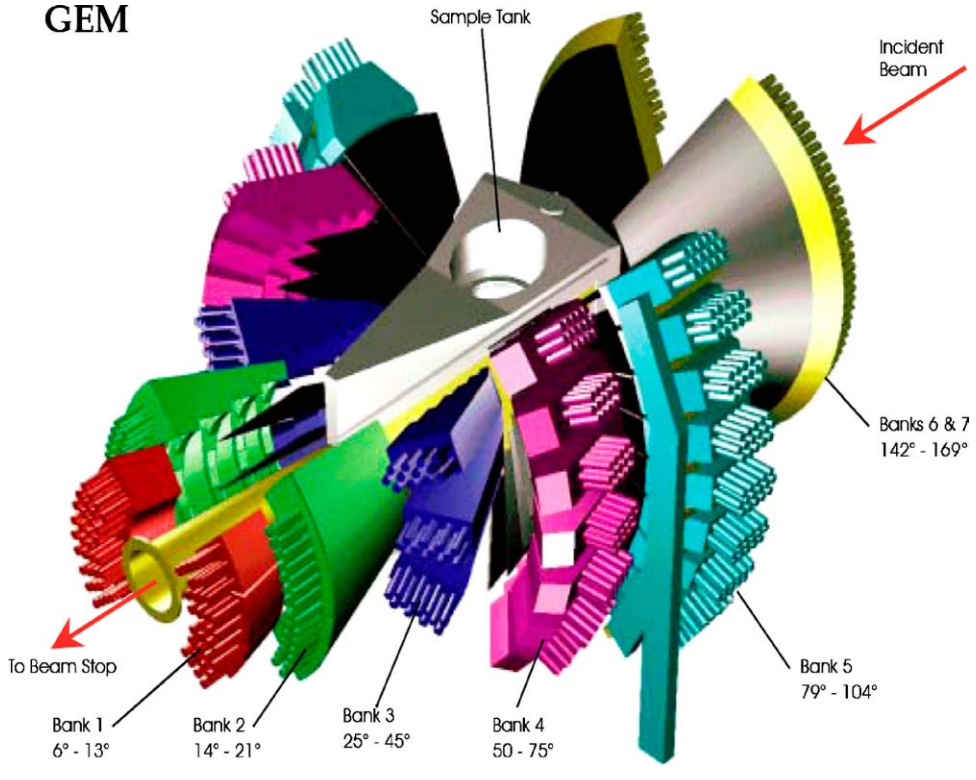

Figure 5 The GEM spectrometer at the ISIS pulsed-neutron source [16].

an energy dispersive technique, where each detector measures a complete diffraction pattern at a fixed angle. Although it is possible to use a single detector, to reduce counting times modern instrumentation covers as much of the solid angle around the sample position as possible. An excellent example of this is the GEM spectrometer at the ISIS pulse neutron source (Fig. 5) [16] which has 3.5 Sr of detector, and is able to take high quality data over a very wide range of *d*-spacings in a few minutes.

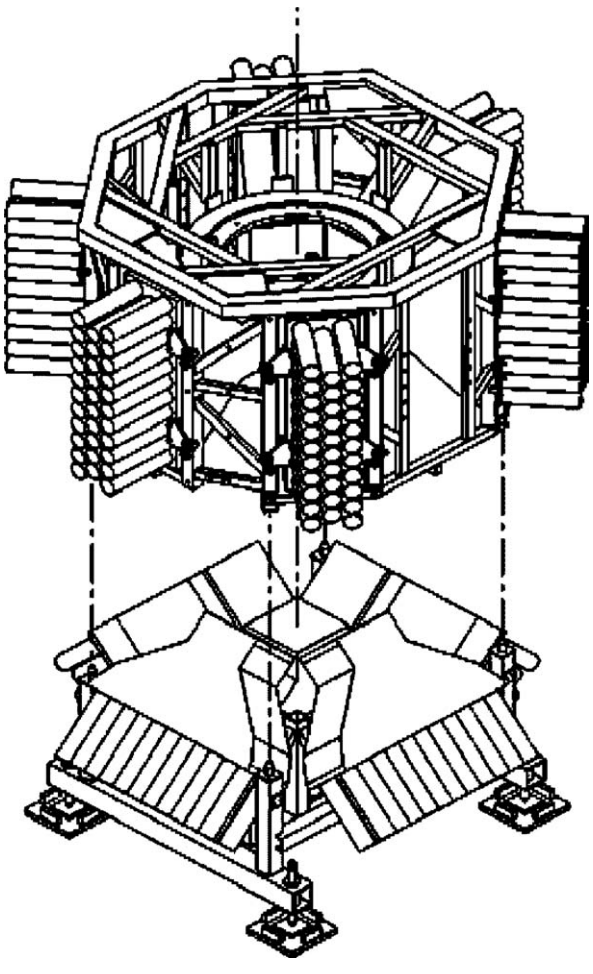

Figure 6 Layout of the D10 diffractometer at the ILL, a typical of a four circle neutron diffractometer [5].

Both D20 and GEM are excellent general purpose diffractometers able to make measurements quickly. If there is a difference, it is that D20 has more flux on the sample and can make measurement more quickly, but at the cost of a slightly lower resolution and smaller *d*-spacing range.

4.1.2. Instruments for single crystal diffraction

The single crystal diffractometer D10 at the ILL (Fig. 6) is a flexible instrument that operates on the same principle as D20; by monochromating the incident beam using a crystal. It has two detectors; one single well collimated detector and one which is large and position sensitive. The single detector has energy analysis which also reduces background and makes it possible to look for subtle effects such as Huang or diffuse scattering or weak satellite reflections. D10 is designed for long wavelengths, between 1.1 and 6 Å.

Single crystal diffraction at a pulsed source is quite different from that at a reactor. The beam incident on the sample is polychromatic; this, combined with large position sensitive area detectors, produces a three dimensional data volume with two positional and one time-of-flight axis. If the area detector is large enough then it is possible to map a complete diffraction pattern from a crystal with a minimal number of orientations. The SXD diffractometer at ISIS (Fig. 7) has detectors covering over 50% of the solid angle. It is able to collect data on typical neutron sized crystals ($\sim$1 cm^3) in a matter of minutes or alternatively small capillary mounted crystals ($\sim$1 mm^3) in several hours. With its ability to map vast areas of the reciprocal lattice, time-of-flight single crystal diffraction is an excellent survey technique, where serendipitous discoveries are more likely.

4.1.3. Solving structures

Solving novel structures is normally the province of single crystal X-ray measurements, and is usually done with X-rays. But for some materials, particularly new

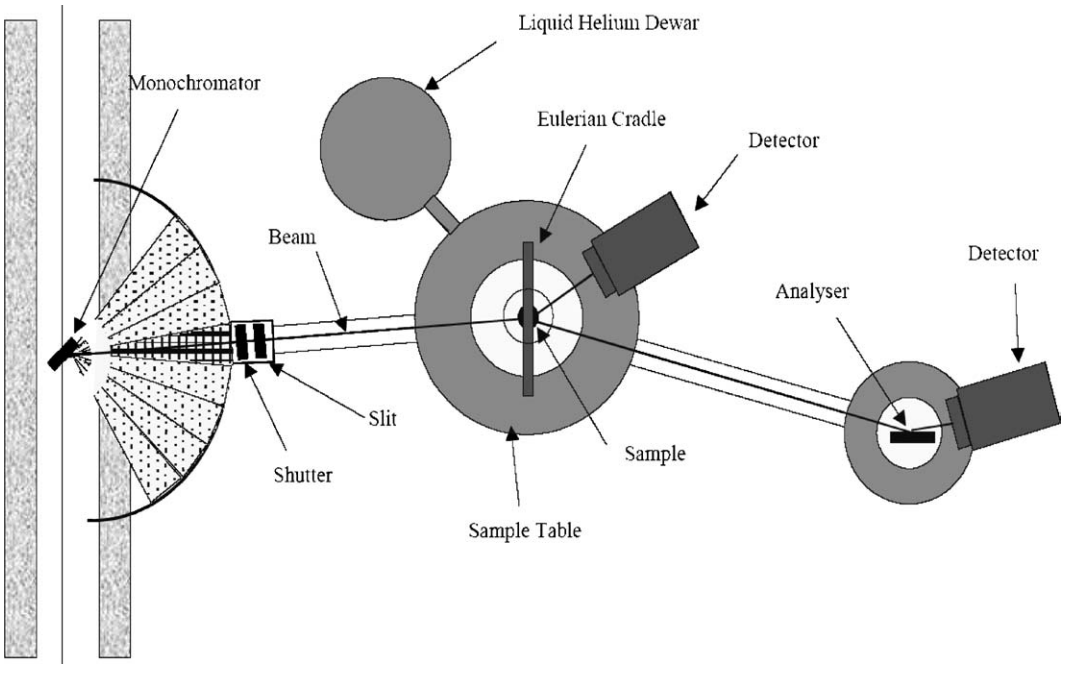

Figure 7 The SXD diffractometer at ISIS has 11 position sensitive detectors arranged in a sphere around sample covering over 50% of the solid angle [6].

ones, or ones created in extreme environments, single crystals are not available, and it is necessary to attempt a solution from powder or polycrystalline data. This is a specialised field but it is becoming increasingly common primarily due to powerful new computational methods [17, 18]. Neutron scattering is a flux limited technique and samples of several 100's of milligram's are usually needed to be able to collect sufficient statistics for a structural solution. Thus neutrons are usually only used as a last resort in cases where X-rays struggle, such as finding the positions of light atoms like as oxygen or hydrogen in the presence of heavier ones, or for magnetic systems.

4.1.3.1. Superconductors. One famous example of this is the refinement of the structure of the high temperature superconductor $YBa_2Cu_3O_{6.8}$. Structural refinement using single crystal X-ray data where not able to accurately determine the oxygen positions [19] and hence failed to get the correct space group. Using high resolution neutron scattering on a powder sample David *et al.* [20] were able to observe the arrangement of the oxygen defects and correctly determine and that the space group was in fact orthorhombic and not tetragonal. The increasing power of Rietveld refinement software now makes it possible to do simultaneous refinement of powder X-ray and neutron scattering data [21]. This technique was used to confirm the structure of $YBa_2Cu_3O_{6.9}$ [22].

4.1.3.2. Ceramic proton conductors. Another important set of examples of the use of neutron diffraction are the ABO_3 perovskites, which when doped with rare-earth ions can be used as proton conductors in devices such as fuel cells. Traditionally, oxide ion conductors based on yttrium stabilized zirconia's (ZrO_2, CeO_2 and $LaGaO_2$ or one of the pyrochlores) are used as separator materials in solid oxide fuel cells (SOFCs). However, the high activation energy of their conductivity means that they require temperatures in excess of 1000°C to operate effectively. Although this technology is well established, fuel efficiencies are lower than they could be and there are problems with material stability at these high temperatures. Proton conducting oxides [23, 24] may be able to replace the oxygen conductors and thus considerably reduce operating temperatures.

In recently years a large amount of work has focused on $BaCeO_3$ and $BaZrO_3$ where the proton mobilities are particularly high. Doping these materials with trivalent rare-earth ions produces vacancies that can accommodate OH^- ions. When these materials are heated in the presence of water vapour the water molecules are dissolved dissociatively; one proton attaching itself to an oxygen atom in the material and the remaining OH^- ion occupying an oxygen vacancy.

The heavy atoms in these materials occupy sites of high pseudosymmetry, which makes detailed structural refinements all but impossible with X-ray diffraction. By contrast the sensitivity of neutron diffraction to both the light atom positions and site occupancies have meant the majority of the structural work on these materials have been done with neutrons [25]. Fig. 8 shows

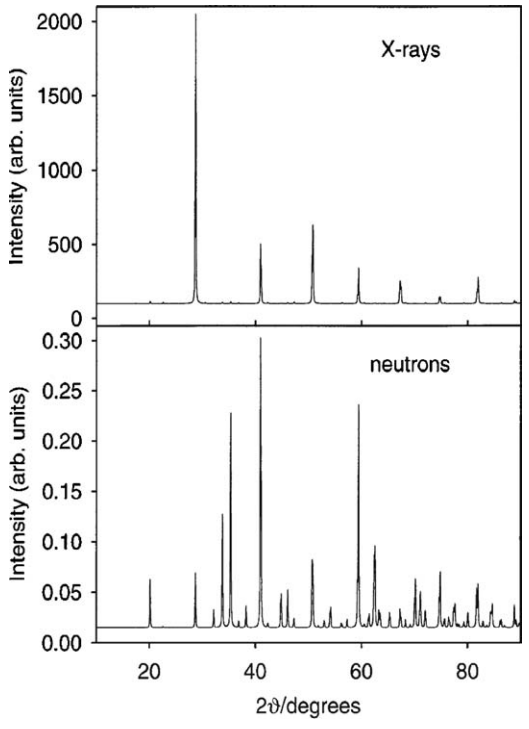

Figure 8 Simulations of the X-ray and neutron diffraction patterns of $BaCeO_3$ at a wavelength of 1.54 Å based on the room temperature structure model of Knight and Bonanos [32].

simulated powder diffraction patterns from orthorhombic $BaCeO_3$ for both X-rays and neutrons. The simulation not only demonstrates the dearth of information in the X-ray pattern, but also the fact that in the neutron data it is possible to observe the small superlattice peaks even at short d-spacings due to the lack of a form factor. The difficulties of finding the correct space group in these materials are compounded by the poor quality of the single crystals, which has meant that the work is done almost exclusively on powder samples. The splitting of the fundamental peaks are also very small and require high resolution neutron data from instruments such as HRPD at the ISIS spallation source which has a $\Delta d/d = 8 \times 10^{-4}$. There have been many attempts to find the correct room temperature space group for Y doped $BaCeO_3$ and this history can be found in the review by Knight [25]. But it is now widely accepted that the correct space groups were conclusively determined by Knight and Bonanos using HRPD [26].

This is of more than simply academic interest; the highest mobilities in these materials are found in the ones whose symmetry is closest to cubic. Large orthorhombic distortions split the single cubic oxygen site into two [27, 28]. These different sites have different binding energies for the proton which increases the activation energy for proton mobility and restrict the proton diffusion path to one dimension.

Another one of the keys issue with these materials is the location of the hydrogen. As was discussed in Section 2.3, hydrogen has a large cross-section for neutron scattering and can easily be seen in the presence of neighbouring heavier atoms. However, the large incoherent cross-section for hydrogen means that it is normally necessary to replace the hydrogen with deuterium to be able to get a recognisable diffraction

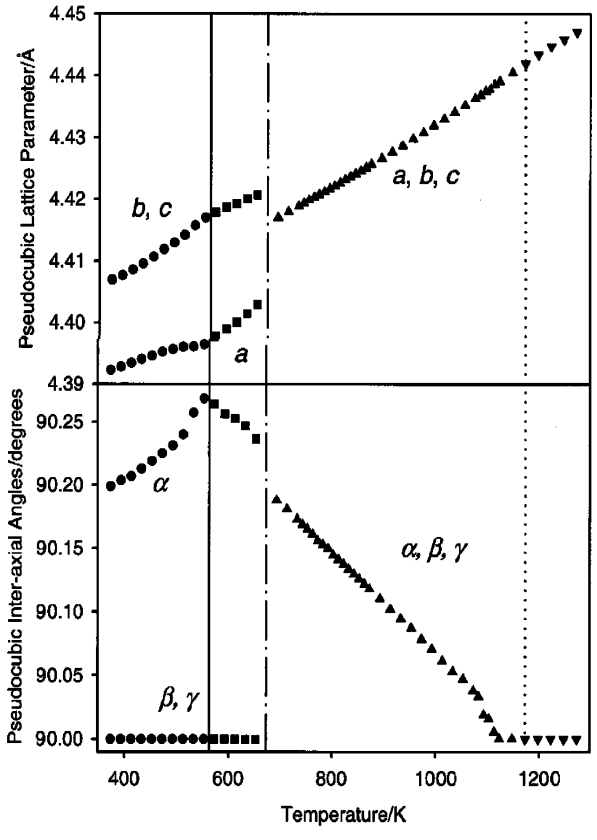

Figure 9 The pseudocubic lattice constants of $BaCeO_3$. Phase *Pmcn* is shown as black circles, *Incn* as black squares, with the phase boundary being shown as a vertical black line. The first order transition between *Incn* and $F3\bar{2}/n$ is shown by a dot-dash line and the $F3\bar{2}/n$ as upward black triangles. The transition to the aristotype is shown by a dotted line, with the $Pm\bar{3}m$ phase shown as downward pointed black triangles [25].

pattern from a powder sample. But this is not the case for materials where the hydrogen concentration is only a few percent. Here it is possible to exploit the change in sign of the scattering length of the two isotopes ($b = 6.671$ fm for hydrogen and $b = -3.739$ fm for deuterium) to create Fourier difference nuclear density maps, in which hydrogen and deuterium should produce positive and negative peaks at the same position. By using this technique Knight [29] where able to determine the hydrogen position in a sample of Y doped $BaCeO_3$. He found that the hydrogen does not sit directly on the O–O bond but is pushed slight outside the octahedron, a result consistent with ab-initio simulations [30, 31].

It is also important to know how the structure of the $BaCeO_3$ changes with the addition of dopants [32, 29], protons [33], and the sequence of phase changes that occur as the sample is heated. Not only could this affect the operation of a device based on these materials, it also has an impact on the methods used to manufacture these materials. An example of this is shown in Fig. 9 [25].

4.1.3.3. Glasses. This wide dynamic range is also important in the study of the structure of glasses. The lack of long range order in glasses means that there is no Bragg scattering only a smooth function *S(Q)* that is related to the Fourier transform of the pair distribution function. To achieve high accuracy in the relative atomic positions it is necessary to be able to measure the total scattering to large values of Q [34], which often best achieved using a pulsed neutron source.

4.1.3.4. Magnetic structures (colossal magnetoresistance). One area in which neutron scattering is almost unique is the determination of magnetic structures. Although various X-ray techniques are being developed they are still not able to challenge the dominance of neutron scattering in the study of the microscopic origin magnetic phenomenon.

The existence of antiferromagnetism was first suggested by Néel in 1932 [35], but it took until 1950's and the development of neutron diffraction by Shull and Wollan for it to be confirmed unambiguously in experiments on MnO [12]. Over the next few years the technique was developed and the structure of various antiferromagnetic and ferromagnetic magnetic materials were solved by the Oak Ridge team [36, 37].

One of the earliest series of magnetic compounds to be studied systematically with neutron scattering where the doped cubic perovskites of the form $La_{1-x}Ca_xMnO_3$ [38]. The interest in these ceramics stemmed from their complex magnetic phase diagram and the dramatic drop in resistivity observed at the paramagnetic to ferromagnetic phase transition [39, 40]. The end members of the series $LaMnO_3$ and $CaMnO_3$ have an antiferromagnetic ground state where the spins on the Mn^{4+} ions interact through the oxygen p-orbitals via the superexchange interaction, but at intermediate concentrations $x \approx 0.2$–0.4 the ground state becomes ferromagnetic. Interest in the doped perovskite manganites $R_{1-x}X_sMnO_3$ (R = La, Pr, Nd and X = Ca, Ba, Sr, Pb) was revived more recently [41] when it was realised that these materials and could be used as sensitive, electrically readable magnetic-field sensors for magnetic memory applications.

The effect has been dubbed 'Colossal Magnetoresistance,' mostly to distinguish it from the 'Giant Mangnetoresistance' effects seen in thin film multilayers and cluster-alloy compounds. It usually explained by the double-exchange theory [42–44], where the Mn 3*d* orbitals are split into localized t_{2g} orbitals and higher energy e_g orbitals. The electrons in the e_g orbitals can be itinerant, and, depending on the relative orientations of the spins on the two sites, can hop from one Mn site to another. An antiferromagnetic arrangement of spins imposes a large energy penalty for this jump, which qualitatively explains why these materials are metallic ferromagnets, and why the resistivity spectacularly increases above T_c.

Although this is almost certainly part of the explanation, it is not sufficient to explain the high resistivity in the paramagnetic state. This led Millis to postulate the formation of polarons due to a strong electron-phonon coupling from the Jahn-Teller distortion around the M^{3+} ions [45]. Millis pointed that these polarons are dynamic and hence incoherent and the clearest signal of their presence would be a discontinuity in the root mean square displacement of the oxygen atoms at T_c. The sensitivity of neutron diffraction to the oxygen made it possible see this discontinuity in $La_{1-x}Ca_xMnO_3$ at

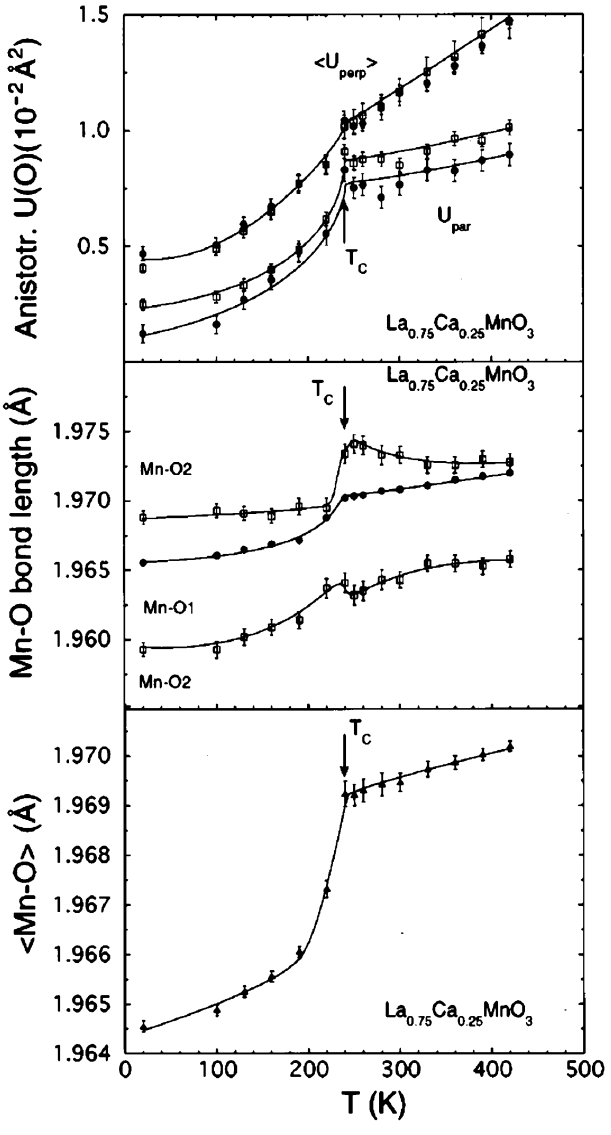

Figure 10 The distortions of the MnO_6 octahedra versus temperature for $La_{0.75}Ca_{0.25}MnO_3$. The average Mn—O bond length (lower), individual bond lengths (center) and projections of the oxygen anisotropic Debye-Waller factors parallel (U_{par}) and perpendicular ($\langle U_{perp} \rangle$) to the diredction of the Mn—O bond lengths for the O1 (filled circles) and O2 (open circles) (upper) [47].

$x = 0.35$ [46] and $x = 0.25$ (Fig. 10) [47]. In the second of these papers Radaelli *et al.* were also able to observe static distortions of the MnO_6 octahedra with a coherence length around 2000 Å. By studying a large number of systems, they were able to show that the disappearance of the static and dynamic distortions occurs at the transition to the metallic ferromagnet. This is consistent with the Millis conjecture, but also with charge ordering of the Mn^{4+} polarons.

Apart from these three-dimensional materials there are also a series of naturally layered manganites where the reduced dimensionality enhances the CMR effect close to the three-dimensional ordering temperature, albeit at the cost of a reduced curie temperature ($T_c \sim$ 100–120 K [48, 49]). $La_{2-2x}Sr_{1+2x}MnO_7$ is made up of two sheets of MnO_2 octahedra separated by a (La, $Sr)_2O_2$ layer, and with a doping of $x = 0.3$ the material becomes a metallic ferromagnet below 90 K. What is interesting is that unlike the three-dimensional manganites this material still shows significant magnetoresistance in the low-temperature metallic phase. And whereas the CMR effect near T_c requires high magnetic fields, here the material saturate in fields as low as 0.1 T. By performing neutron diffraction in an applied magnetic field on samples at low temperatures [50] it was possible to show that the origin of this effect was very similar to that in the layered GMR systems. At zero applied field the coupling within the bilayers is ferromagnetic and hence metallic, but antiferromagnetic along the *c*-axis; but in an applied field this *c*-axis coupling becomes ferromagnetic, allowing electron tunnelling between the MnO bilayers.

In these systems the neutrons ability to solve magnetic structures, its sensitivity to the position of the oxygen atom's position and the ability to do diffraction in extreme environments (in this case high magnetic fields) have made it possible to begin to understand the microscopic origin of the magnetoresistance. Many of the more challenging problems in contemporary condensed matter physics are those, like the manganites, whose complex behaviour stem from a strong coupling between the lattice, charge, spin and perhaps orbital degrees of freedom. The unique properties of neutrons mean that neutron scattering techniques are playing a central role in unravelling the physics of these fascinating systems.

4.1.4. Non destructive measurements

The highly penetrating nature of neutrons makes it possible to perform truly non-destructive analysis. This is crucial for precious and/or unique archaeological specimens or for studying engineering components in the form that they will ultimately be used.

4.1.4.1. Archeometry. Ceramic fragments are almost indestructible and are found at almost all archaeological sites. The examination of archaeological ceramics to date a site or understand trading patterns and cultural exchange is of fundamental importance to archaeology. Neutron diffraction can be used to accurately measure the mineral phase abundance in clay or pottery products, producing a unique fingerprint that can be used to classify an object.

The most frequently used techniques for archeometric characterisation of ceramics are element specific such as electron microprobe analysis, X-ray florescence, neutron activation and plasma atomic emission spectroscopy. However, most of these techniques are invasive and require destructive sampling such as coring, cutting or even powdering of some portion of the object under investigation. X-ray diffraction is often used and, like neutron diffraction, it is able to identify the crystalline phases within the object, but it requires a sample to be extracted and powdered. Samples for neutron scattering measurements do not need to be pre-prepared; fragments or even whole samples can be studied with relative ease. It is also insensitive to the surface and can look through patinas, corrosion layers or decorative coatings to the ceramic below. A dispersive technique, like time-of-flight neutron diffraction, has certain benefits over angular dependent measurements particularly for studying intact items, since it is

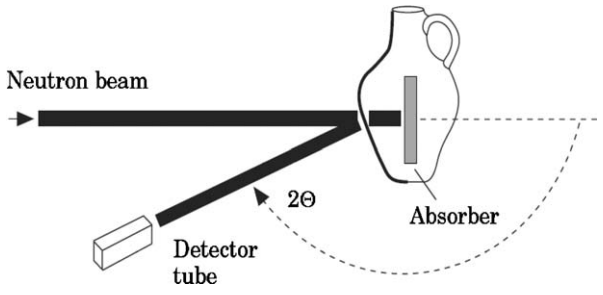

Figure 11 A schematic of the layout used in measuring archaeological pottery using time-of-flight neutron diffraction.

possible to measure a complete diffraction pattern over a very wide *d*-spacing range at a fixed angle (Fig. 11).

Böttger style pottery was first made in Saxony in 1707 as a copy of 4000 year old Chinese Yixing stoneware, and become popular in 17th century Netherlands and 18th century England. This kind of stoneware is highly valued on the international arts market and, consequently, some objects are thought to be forged. By performing a mineral phase analysis using time-of-flight neutron scattering, Kockelmann *et al.* [51] were able to create a fingerprinting technique to distinguish between English, Dutch and Chinese pottery and potentially identify anomalous objects that do not fit into these categories. Pottery is a complex mix of crystalline and glassy components, whose phase fraction depend on the source clay and firing temperature. The red colouring in Böttger stoneware comes from antiferromagnetic hematite. The major phase is quartz but other phases present include mullite and cristobalite which form at firing temperatures above 1000°C, and vitreous SiO_2 which begins to appear at even higher temperatures [52, 53]. By creating a phase space based on the ratios of the phase fractions, it is possible to identify groupings corresponding to the major types and also identify outliers which are potentially forgeries.

4.1.5. Extreme sample environments

The low attenuation of neutron beams in most materials make the design and operation extreme sample environment equipment on neutron beam lines relatively straightforward.

4.1.5.1. High pressures. In the past, diffraction measurements at high pressures have been the preserve of synchrotron X-ray sources using diamond anvil cells. But the recent development of high volume pressure cells such as the Paris-Edinburgh cells [4] has allowed considerable progress particularly areas such as high-pressure mineralogy [54]. These cells allow sample volumes of 90 mm^3 and with the use of sintered diamond anvils can routinely achieve 25 GPa, although 40 GPa is possible using a double-toroidal $Ti_{66}Zr_{34}$ gasket. Most of this work is done at room temperature or below, but the recent development of an internally heated cell makes it possible to perform experiments at high temperatures and pressures [55], with the current state of the art standing at 7 GPa and 1500°C.

These kinds of hydrostatic pressure measurements can be used to extract bulk modulus or Gruneisen parameters, but are more often used to search P-T space for new phases. Diffraction under uni-axial stress is also becoming more common as equipment improves. Such measurements make it possible to extract Young's modulus, Poisson ratios, and elastic compliances by observing the shifts in the Bragg peaks as a function of applied stress. But because of the problem with surface stress/strain gradients this kind of work is better done with neutrons or high energy synchrotron X-rays. Although traditionally done on single crystals, it also possible to extract single crystal compliances from polycrystalline and even multi-phase materials as long as the Bragg reflections are sufficiently isolated [56], and has been used to extract the compliances in tetragonal zirconia [57].

4.1.5.2. Toughened zirconia. Although ceramics are well known for their strength and hardness; they are typically brittle, which is of concern in applications in which they are subjected to mechanical or thermal shock. However, some ceramics, notably polymorphs of zirconia, do have considerable fracture toughness [58, 59]. Pure zirconia has three ambient pressure polymorphs: a cubic form (*c*) at temperatures above 2640 K, a tetragonal form (*t*) between 1400 and 2640 K, and a monoclinic form (*m*) below 1440 K. Because the oxygens play the dominant role during these transformations neutron scattering is often used to characterise these phases [60], especially since the measurements are routinely done at very high temperatures. More recent work has focused on the detailed nature of the phase transitions, in particular the tetragonal to monoclinic transition, which is first order and thought to be displacive in character. Although no-soft mode has actually been observed; neutron diffraction has shown that oxygen anisotropic temperature factors are consistent with the soft-mode formalism [61]. These high temperature forms can be stabilised at room temperature by doping with di- or tri-valent metal ion oxides and show remarkable toughness due to their resistance to crack propagation. The mechanism responsible for the toughness of the tetragonal zirconia polycrystals (TZP) is thought to a martensitic tetragonal-to-monoclinic transformation induced by the stress field at a crack tip. The increase in volume and shear forces that occur at this transition relieve the stress and hinder propagation of the crack [62, 63]. However, this cannot completely account for the toughness of these ceramics, particularly at high temperatures. And it was postulated that they might also exhibit a ferroelastic transition in the presence of an external stress [64–66]. This was unequivocally demonstrated by neutron diffraction measurements performed under uni-axial pressure [67]. A fully tetragonal yttria doped zirconia (3 mol% Y_2O_3) was seen to undergo reversible tetragonal domain switching above a coercive stress of around 1.6 GPa.

4.1.5.3. Hydrothermal processing. Although the use of X-ray diffraction techniques for following hydrothermal crystallisations *in situ,* have been available for several years, these techniques do not work well for strongly absorbing materials. Recently Walton *et al.* [68] developed a hydrothermal cell for use with

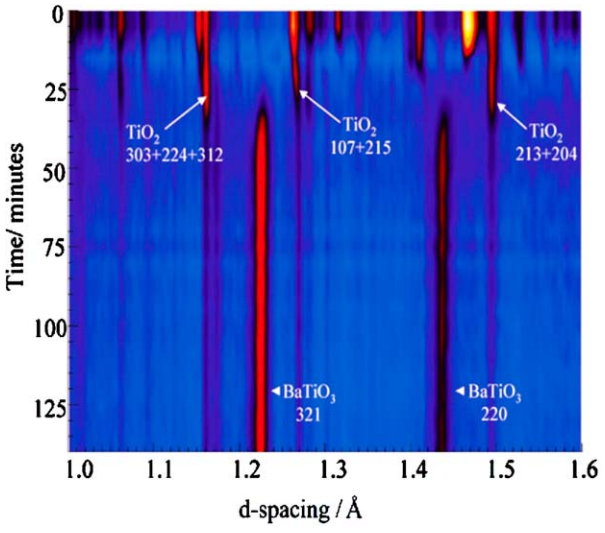

Figure 12 A contour map of the diffractions patterns from the ISIS hydrothermal on GEM diffractometer spectrometer. It is possible to see the decay of the TiO_2 peaks and the growth of the $BaTiO_3$ as a function of time [69].

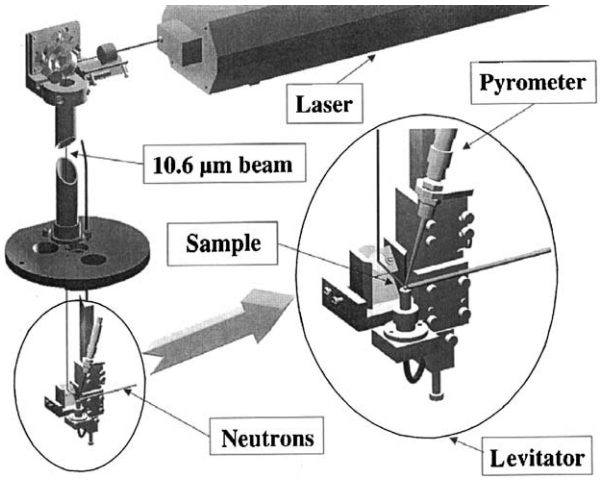

Figure 13 The levitation kit used to measure the structure of molten alumina [71].

neutrons and were able to measure corrosive and/or reactive chemicals at temperatures up to 250°C. In an interesting series of experiments [69] they were able to watch the crystallisation of barium titanate ($BaTiO_3$) from a solution of Ba and Ti precursors at a range of temperatures. Diffraction patterns where taken at 5 min on the GEM diffractometer at ISIS, and from this data it was possible to see the disappearance of the precursor chemicals and watch the crystallisation of the $BaTiO_3$. Not only were they able to understand the rate limiting chemical process, but because they were doing full Rietveld refinement for each measurement, they were also able to pull out additional information such as the particle size.

Hydrothermal processing is of great commercial interest, not only is it possible to manufacture ceramics at lower temperatures, and hence more cheaply. It is also possible to control the morphology of the final material for cases where fine powders are needed for the preparation of ceramics with few grain boundaries after sintering and for the chemical fabrication of miniature devices. One of the problems with hydrothermal processing is that it is somewhat of a 'black-art', where the results depend on a number of control parameters: temperature, precursor chemicals, pressure etc. *In-situ* measurements are an efficient way of mapping out this phase space to optimise the reaction conditions.

4.1.5.4. High temperatures. High temperature studies with neutrons are relatively straightforward and furnaces that operate at temperatures up to 1700°C are used routinely, making it possible to study the formation of ceramics under conditions similar to those used commercially. There are a large number of studies of this kind; the one chosen for illustration here demonstrates the value of the quantitative analysis that is possible with Rietveld refinement.

Partially stabilised Zirconia is an important engineering ceramic, whose properties depend on a carefully controlled heat treatment. It is first fired at 1700°C and then heat treated at 1100°C for several hours. Its toughness is dependent on a stress-induced martensitic transformation from tetragonal to monoclinic, and so the optimisation of the tetragonal volume fraction is the key to optimising its performance. In a neutron diffraction study of the aging process of magnesia stabilised zirconia, Argyriou *et al.* [70] were able to follow the aging of the fired material at 1100°C and watch the development of the tetragonal volume fraction during the cooling process. From refinement, the volume fractions and lattice parameters of the five separate phases where extracted. It was also possible to watch the growth of the internal strain in the tetragonal phase due to morphology of the grains and the change in a/c ratio indicating that the MgO stabiliser was lost during in the aging process.

For temperatures above 2000 K, finding a crucible to contain samples becomes problematic. Apart from the fact that few materials are still solid, problems are also caused by the increased reactivity of most materials at elevated temperatures. Recently, aerodynamic contactlesss levitation techniques, in which a laser is used to melt the sample, have been developed for use with NMR and X-ray scattering. This equipment was also used to study molten alumina at 2473 K using neutron diffraction [71]. By fitting the data using a model that includes empirical potentials it was possible to show that the liquid still has significant chemical bonding. This model was also able to accurately reproduce previously measured X-ray diffraction data [72].

4.1.5.5. Electrolysis lithium batteries. In most commercial lithium-ion batteries the cathodes are made from $LiCoO_2$. It has a high electrode potential of around 4 V, its layered rock-salt structure allows for fast lithium diffusion and it is relatively stable against the removal and addition of lithium [73]. However, cobalt is toxic and expensive, which has prompted the search for replacement materials. Some of the most promising are those based on manganese; it is less than 1% of the cost of cobalt and far less toxic. Two classes of materials exist; one with a spinel structure based on the formula $LiMn_2O_4$ [74], and another based on $LiMnO_2$ [75] with a layered rock salt structure isostructural to $LiCoO_2$. Both these materials have been intensively

investigated with both X-ray and neutron diffraction. The X-rays are generally used to look for phase changes associated with the disintercalation process and lattice damage and/or changes in particle size due to the cycling of the lithium. However, the lithium position and occupancies are difficult to refine with X-rays and this is more commonly done with neutrons. The major technological issue with all these materials is their structural stability. The pure spinel $LiMn_2O_4$ is unstable due to a Jahn-Teller distortion of the $Mn^{3+}O_6$ octahedra which forces a large cubic to tetragonal phase transformation during the discharge process which destroys the structural integrity of the electrodes, and limits their practical charge capacity. The study of the atomic structure of the cathode is then central to finding strategies to combat this problem and very many X-ray and neutron studies have been done to looking at doped variants to change the manganese valence and suppress the transition [see references in [73]]. In most of these studies it is sufficient to look at an electrode after cycling, but *in-situ* X-ray [76] and neutron [77] diffraction studies are increasingly common, and provide direct methods for looking at the mechanisms of this process in detail. The layered manganese structures also suffer from structural instabilities and transform to the spinel structure after cycling. A large number of diffraction studies, using both neutrons and X-rays, are currently underway to understand the effects of doping with transition metals [see references in [78]].

4.2. Inelastic neutron scattering

Often knowing the atomic structure of a material will be sufficient to understand its nature. But to gain a deeper insight into the underlying physics of say a phase change, it is necessary to also understand the atomic dynamics. The vibrational motion of atoms is, entirely or in part, responsible for a large number of the characteristic properties of a material, such as the specific heat, thermal conductivity, optical and dielectric properties and electrical resistance, but it is also a direct way of understanding the nature of atomic bonding. And with the current interest in smart or functional materials whose properties are often determined by a complex balance or strong coupling between competing phenomena, understanding the atomic and magnetic dynamics is essential.

The most commonly used spectroscopies are the light scattering techniques: Raman and infrared. Compared to neutron scattering they are cheap, readily available and highly sensitive. But they do have certain limitations: They can only measure near the Brillouin zone centre and are only sensitive to certain vibrational modes. The calculation of the scattered intensity is also difficult and prone to error and so information is usually only taken from the positions of the observed modes. However, the simplicity and sensitivity of the techniques means that they are often used to identify or 'finger print' compounds something that is rarely done with neutrons. Inelastic neutron scattering is usually used to understand the physics of a system. It is a highly quantitative probe whose results are directly comparable to numerical and analytical calculation. It can be used to understand the nature of a phase transitions or linked directly to thermodynamics quantities, like specific heat or thermal conductivity, or structural properties such as force tensors or bulk and shear moduli.

It is still one of the few methods available to measure phonon and magnon dispersion curves. And, due to the unique nature in way that hydrogen scatters neutrons, it is a natural technique for measuring the vibration or diffusion of hydrogen in a material.

4.2.1. Instrumentation

The triple-axis spectrometer is a powerful and versatile instrument, and it is also one of the oldest; developed in the early 1950's by Brockhouse at the Chalk River reactor in Canada [79]. His famous C5 triple-axis spectrometer, immortalised in Kittel's 'Introduction to Solid State Physics', proved to be an enduring design and it is possible to find similar machines on reactors today. Using this machine Brockhouse and his team made a series of seminal experiments including the first measurement of phonon dispersion curves [80], the observation of the first magnon dispersion in magnetite [81], crystal field splitting [82], Kohn anomalies [83] and many others. This work rightly lead Brockhouse sharing the 1994 Nobel Prize for Physics with Clifford Shull.

A triple axis spectrometer uses a single crystal to monochromate, and define the direction of, the neutrons incident onto the sample. And an analyser crystal plays a similar role for the scattered neutrons. In this way it is possible to measure the scattered intensity at any energy or momentum transfer so that the experimenter can set up scans through the Brillouin in any direction. This is a very versatile technique and makes it possible to measure the dispersion and polarisation of an excitation in any crystal direction in an accurate and controlled way. A typical triple-axis machine is shown in Fig. 14.

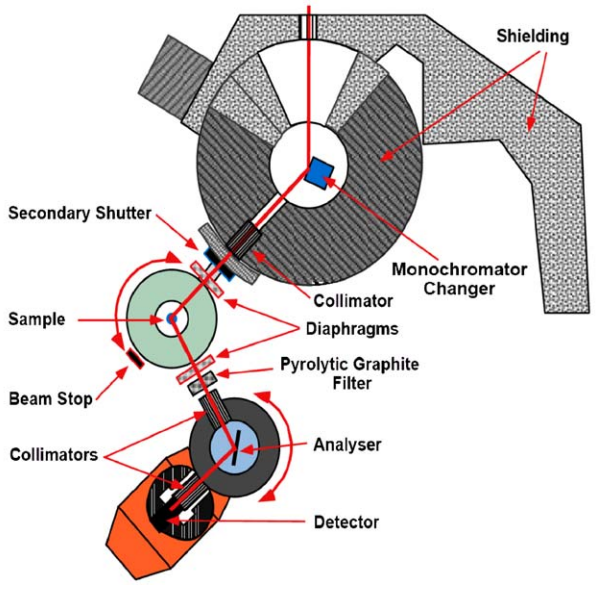

Figure 14 The IN3 Cold triple-axis spectrometer at the Institute Laue Langevin in France. The white incoming beam is monochromated using Bragg reflection before hitting the sample. The scattered beam is intercepted by an analyser filter at an angle 2θ, before being detected. By changing the monochromator, sample and analyser angles it is possible to do a point by point measurement along any trajectory in the accessible momentum and energy transfer space [5].

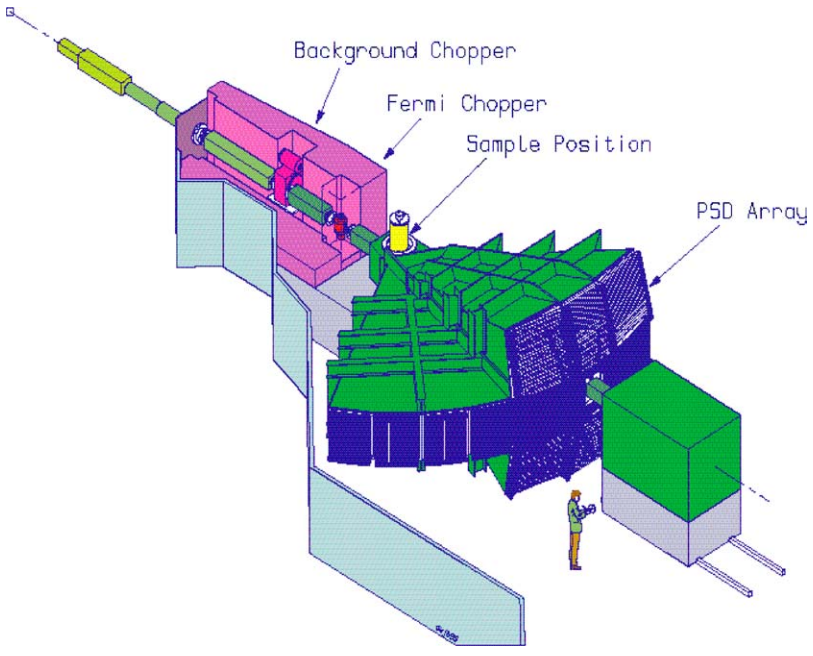

Figure 15 The MAPS spectrometer at the ISIS pulsed neutron source showing the large position sensitive detector array (PSD's) [6].

A pulsed source has considerably less time averaged flux then a reactor. Instruments on such a source can only begin to be competitive when they exploit the time structure of the neutron pulse. There are several ways this can be done, but one kind of spectrometer that is always found on a pulsed source uses a mechanical rotor (known as a 'Fermi chopper') to select a monochromatic pulse of neutrons which are then scattered from the sample to the detectors. By timing the neutrons' total time-of-flight from the source to the detectors it is possible to calculate the change in neutron's velocity at the sample and hence the energy transferred to the sample. A typical instrument of this type can be seen in Fig. 15. In this kind of machine it is not possible to control the position in momentum and energy in the same way as with a triple-axis machine; two of the axis will always be coupled. However, with the latest instruments, which have position sensitive detectors it is possible to map large volumes of the Brillouin zone in a single measurement and make cuts through these volumes in software.

4.2.2. Soft modes

The study of phonons played a central role in the understanding of condensed mater physics during the 1960 and 70's. Many important fundamental concepts were driven by the interplay between inelastic neutron scattering and theory. The suggestion in the late 1950's that several types of solid phase transition might be triggered by instabilities in the normal modes dynamics [84] lead to flood of experimental and theoretical work. If the frequency of a phonon mode decreases, and reaches zero at a finite temperature, then the crystal lattice will become unstable against this mode and a structural phase transition with occur. This 'soft-mode' driven phase transition was first unambiguously demonstrated by Cowley [85] in a transverse optic mode in $SrTiO_3$. The 110 K transition in $SrTiO_3$ was attributed to an instability of a mode at the [111] zone boundary [86] which was then quickly confirmed with neutron scattering measurements [87, 88].

Although this is still an important concept in ferroelectric and piezoelectric materials (see Section 5.2) much current interest in condensed matter physics is focused on the subtle interplay between the lattice and electronic structure of a material, typified in systems like the high temperature superconductors and colossal magnetoresistive materials.

4.2.2.1. Colossal magnetoresistance. The colossal magnetoresistance seen in the manganites has already been discussed in Section 4.1.3.4. Although it is vital to know the magnetic and atomic structure of these materials, it is the dynamics of the spins that gives the most direct link to the theory.

At a doping of $x = 0.3$, $La_{1-x}Pb_xMnO_3$ becomes a metallic ferromagnet. By measuring and fitting the spin wave dispersion Perring *et al.* [89] were able to show that the whole dispersion could be reproduced with a single ferromagnetic nearest-neighbour coupling. This remarkable simplicity is entirely

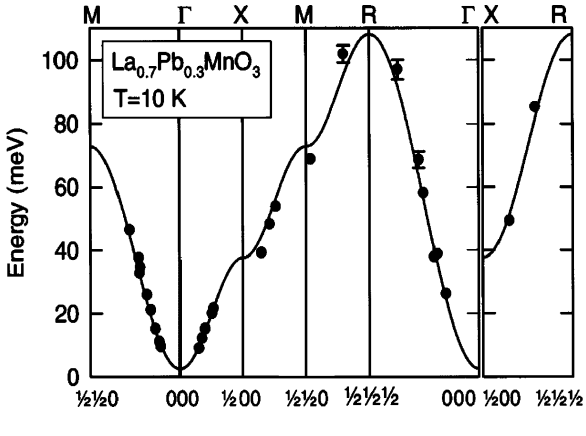

Figure 16 The spin wave dispersion in $La_{0.7}Pb_{0.3}MnO_3$, measured at 10 K on the HET spectrometer at ISIS. The solid shows the dispersion of a Heisenberg ferromagnet with nearest-neighbour coupling [89].

consistent with the double-exchange model [90] normally used to explain the magnetoresitivity in these materials. Similar measurements on other systems show that this simplicity is not common to all these systems as $La_{0.67}Ca_{0.33}MnO_3$ [91], $Pr_{0.63}Sr_{0.37}MnO_3$, $La_{0.7}Ca_{0.3}MnO_3$ and $Nd_{0.7}Sr_{0.3}MnO_3$ [92] and $La_{0.7}Ba_{0.3}MnO_3$ [93] show strong damping at the zone boundary that cannot be described with a double-exchange model. Although there is a suggestion that this difference may be linked to differences in the Curie temperatures at the time of writing the problem is still current and controversial.

Interestingly a study of the bilayer manganites $La_{2-2x}Sr_{1+2x}MnO_7$ for $x = 0.3, 0.35$ and 0.40 [94], has also shown dispersion that can be fitted with a nearest neighbour Heisenberg model, although there is some hardening of the magnons at the zone boundary in the $x = 0.3$ sample.

4.2.2.2. High temperature superconductivity. One of the most active areas in condensed matter physics has been the study of the unconventional superconductivity seen in the ceramic cuprates. This interest is both for reasons of potential application, but also because complexity of the underlying physics is still not understood despite nearly two decades of work.

One of the most important pieces of information needed to understand the origin of superconductivity is the nature of the intermediate boson that provides the attractive interaction between the electrons [95]. In the case of conventional phonon mediated superconductivity, neutron scattering is able to measure phonon spectrum and the strength of the electron-phonon coupling by examining the changes in the phonon lifetimes on entry into the superconducting phase. With these two pieces of experimental information the theory can 'predict' the transition temperature. Neutron scattering has a distinguished history in the study of superconductivity, but the fact that the superconductivity occurs in the vicinity of magnetically ordered phases, has meant that it has taken on a even more pivotal role in the work on the cuprates. The scale of the neutron scattering literature is this field is dauntingly large and it is only possible to present a small flavour of the work here.

$La_{2-x}Sr_xCuO_4$ is the archetypal cuprate consisting of single CuO_2 planes alternating with $La_{2-x}Sr_xO_2$ charge reservoir layers. Shortly after the discovery of superconductivity in the $x = 0.15$ material, Vaknin

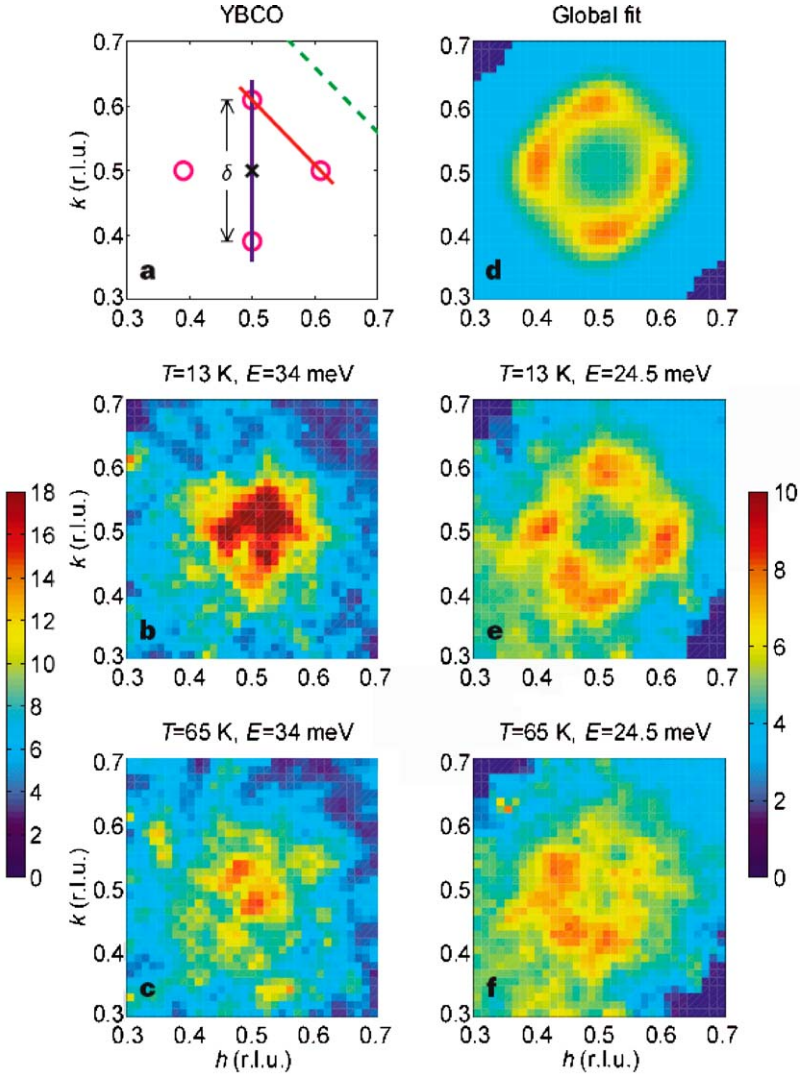

Figure 17 Images of the magnetic excitations near the (1/2, 1/2) reciprocal lattice position in $YBa_2Cu_3O_{6.6}$ ($T_c = 62.7$ K) for an energy transfer of 24 meV. Data were collected using the new PSD array on the HET spectrometer. (Left panel) scattering in the normal state $T = 65$ K. (Right panel) scattering in the superconducting state, $T = 13$ K [98].

et al. [96] discovered antiferromagnetism in the insulating parent compound La_2CuO_4. The unit cell doubles, with each Cu^{2+} ion having opposite spin to its four neighbours, producing a superlattice peak at ($^1/_2$, $^1/_2$) in the reciprocal space of the two-dimensional layer. Once doped into the metallic superconducting regime, this peak disappears, to be replaced by spin fluctuations observed in triple-axis experiments as a quartet of peaks arranged around where the antiferromagnetic peak was in the parent compound [97]. For a long time these incommensurate fluctuations were considered to be a feature of the La_2CuO_4 based compounds, but the discovery of similar excitations in the bilayer cuprate $YBa_2Cu_3O_{6.67}$ [98] imply that they are more general. The incommensurability, widths and scaled (by E/T_c) intensities are indistinguishable from those for similarly doped $La_{2-x}Sr_xCuO_4$ [99, 100].

4.2.3. Hydrogen

Hydrogen has a unique position in neutron scattering; its incoherent cross-section is an order of magnitude larger than that of any other element, this and its large vibrational amplitude mean that it will dominate the scattering from any material that contains it.

At low energy transfers, diffusive motions of the atoms can Doppler broaden the zero energy transfer line (usually called the elastic line) a phenomenon known as Quasi-Elastic Scattering (QENS). At small momentum transfers ($\hbar\boldsymbol{Q}$) the width of this broadening can be modelled with a single Lorentzian which is related to the self-diffusion coefficient D. For a hydrogenous systems the scattering function $S(\boldsymbol{Q}, \omega)$ is a single Lorentzian of width $\Gamma\boldsymbol{Q}$

$$S(\boldsymbol{Q}, \omega) = \frac{\Gamma(\boldsymbol{Q})/\pi}{\Gamma^2(\boldsymbol{Q}) + \omega^2} \tag{7}$$

Which for a polycrystalline sample is given by

$$\Gamma(Q) = DQ^2 \tag{8}$$

At higher momentum transfers, when $\boldsymbol{Q}$ is comparable to the inverse of the interatomic distances; the scattering contains information about the size, and in single crystals, the direction of the diffusive jumps. QENS is a powerful technique for measuring diffusive or rotational motion of all types, not just that of hydrogen. For example the motion of oxygen the zirconia based ceramics used in the high temperature fuel cells is link to its short range order and has been studied extensively using diffuse and Quasi-elastic neutron scattering [101].

At higher energy transfers it is possible to see the vibrational modes of hydrogen. Because the scattering hydrogen is largely incoherent it is not possible to extract information about the dispersion of these modes directly. But since most of the high energy modes are largely dispersonless optic modes, this rarely an issue. These modes give information on the nature of the hydrogen bonding and, when combined with first-principles density functional calculations, is a stringent test of any physical model.

4.2.3.1. Proton conducting oxides. Quasi-elastic neutron scattering has played a central role in understanding the nature of the proton diffusivity in the ABO_3 type proton conducting oxides (see Section 4.1.3.2). Most of the initial work was done by Hemplemann *et al.* [102, 103] on polycrystalline samples of $SrCe_{0.95}Yb_{0.05}H_{0.02}O_{2.985}$. In the oxides each proton covalently bonds to an O^{2-} ion forming an OH^- ion. If the O $\cdots$ O distance is short enough a bridging hydrogen bond will also form, making it possible for the hydrogen to hop from one O^{2-} ion to another

$$\text{O—H}\cdots\text{O} \leftrightarrow \text{O}\cdots\text{H—O} \tag{9}$$

If the OH^- ion is able to rotate then long range hydrogen diffusion is possible. This mechanism was first suggested nearly 200 years ago to explain the high ionic conductivity of H^+ in aqueous electrolytes and is called the Grotthaus mechanism [104]. But it also appears to be the basis of the proton conductivity in these oxides.

The Quasi-elastic data is made up of three separate Lorentzians with very different widths requiring measurements over a wide range of energies. Two instruments were required to cover this range: the high resolution spectrometer IRIS at the ISIS spallation source (4.2 μeV resolution), and the triple axis spectrometer E7 (1 meV resolution) at the medium flux reactor of the Hahn-Meitner-Institute. The data is complex but Hempelmann *et al.* [103] were able to use it to develop the Grotthous based model for the hydrogen motions that is now widely accepted. The hydrogen motion is characterised by periods of free diffusion then trapping for a period of time τ_0. Whilst in its free state the OH^- rotates very rapidly, but after about 80 rotations the hydrogen hops to another O^{2-} ion and rotation commences about this new site. From the data at low momentum transfers it is possible to extract the self-diffusion coefficient as a function of temperature, which compares well to the bulk proton conductivity measured with impedance spectroscopy [102]. The higher momentum transfer data gives information about the jump length, making it possible to identify the trapping centres as the aliovalent dopant, in this case Yb. These hypothesis are supported by ab-initio and molecular dynamics calculations on this and other similar systems [105, 106].

Inelastic Neutron Scattering (INS) at higher energies probes the vibrational modes of the hydrogen. This provides a means for mapping the potential that the protons experience. If the dopant ions have a strong trapping effect then this should be reflected in the OH^- vibrational modes. In INS measurements on a series of samples $SrCe_{0.95}M_{0.05}H_xO_{3-\delta}$ (where M = Sc, Ho and Nd) dramatic changes appear in the OH^- bending modes [107]. Thus the bending mode energy appears to increase as the cation size gets smaller (Nd $\rightarrow$ Ho $\rightarrow$ Sc). These are due to changes in the hydrogen potential which have a bearing on the proton jump rate. Using ab-initio calculations of the hydrogen vibrations in supercells of $Sr_8Ce_7ScHO_{24}$, Yildirim *et al.* [108] were able to show that the proton sites around the Sc atoms were indeed energetically favourable due to their

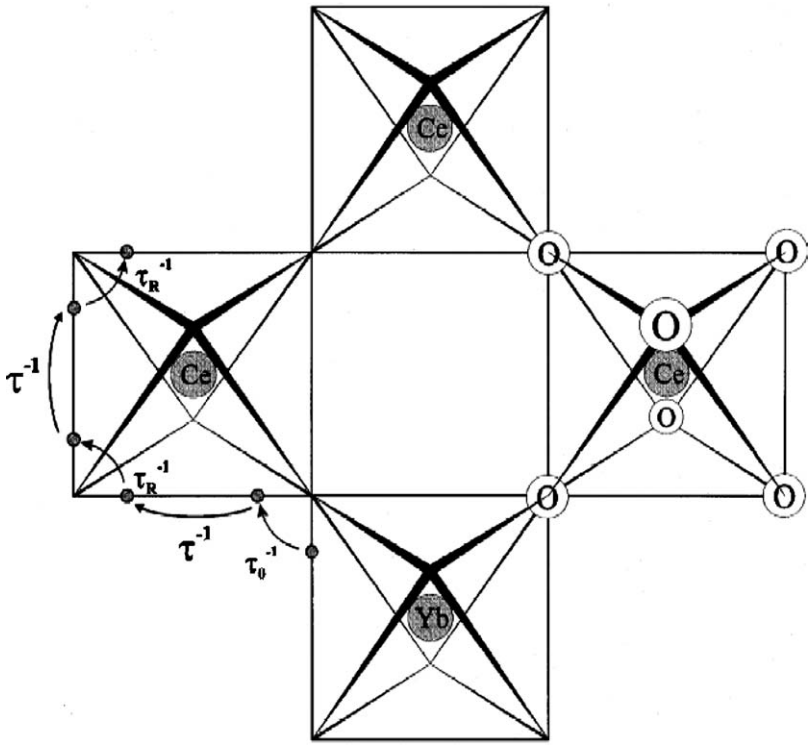

Figure 18 A schematic representation of the proton diffusion mechanism in the proton conducting perovskites. In this case Yb doped $SrCeO_3$. The structure consists of corner sharing oxygen octahedra, with the small cation (Ce^{4+} or the dopant Yb^{3+}) inside the octahedra and the large Sr^{2+} cation located at Z = 1/2 in the centre of the figure. τ_R^{-1} is the hoping rate of the OH^- rotations, τ^{-1} is the hoping rate for jumps between O^{2-}, and τ^{-1} is the escape rate from the vicinity of the dopant ion [103].

difference in charge. This difference is sufficient to change the position of the proton so that although the nearest neighbour oxygen distances are almost the same, the next nearest-neighbour distances are radically different which has a large effect on the OH^- bending mode energies. It appears from the calculations that the mode at 115 meV is due to the protons at the doped (Sc) site and the mode at 80 meV due to those at the undoped (Ce) site. Hence the INS gives an independent way of studying the trapping of the protons.

5. Some case studies

It is interesting to follow some case studies in more detail to see the contribution that neutron scattering can make in some topical problems in ceramics research. No attempt has been made to be balanced or complete in these case studies, they are merely to illustrate some of the points made in previous sections.

5.1. Zirconium tungstate

In 1996 zirconium tungstate (ZrW_2O_8) was demonstrated to have negative thermal expansion from absolute zero to 1050 K [109, 110], the temperature at which it decomposes. Negative thermal expansion is an unusual but not particularly rare phenomenon, and can be observed in, for example, many tetrahedrally bonded materials such as silicon or ice [111]. It usually occurs over a small range of temperatures but in ZrW_2O_8 the negative expansion is linear over a very wide temperature range and is similar in magnitude to the positive expansion of 'normal' ceramics such as Al_2O_3. Negative thermal expansion can be related to a transverse vibration of a single or rigid group of atoms, and is normally described using the 'guitar string' analogy; the transverse motion of a heavy mass suspended between two strings will tend to pull in the string's supports, leading to a contraction. ZrW_2O_8 is an open framework structure consisting of corner-link ZrO_6 polyhedra. A rigid unit rotation of these units, pull in the neighbouring octahdera, thus shrinking the crystal.

In a tour-de-force experiment, on the high resolution powder diffractometer HRPD at the ISIS pulsed neutron source, David *et al.* [112, 113] made a series measurements at 2 K intervals from 2 to 520 K on a 15.7 g powder sample of ZrW_2O_8. Each measurement took approximately 5 min with 2 min allowed to equilibrate the temperature. Each of the 260 measurements was fitted using Rietveld refinement to extract lattice parameters, atom positions, occupations and temperature factors. The lattice parameters were refined to a precision of ± 0.00003 Å and oxygen temperature factors where refined anisotropically. The orientation of the oxygen thermal ellipsoids confirms the very pronounced rigid body vibrations of the constituent polyhedra. The effective fractional bond shortening associated with this polyhedral libration is given by:

$$(\Delta d/d)_{(\mathrm{zr}-o)} = -\langle u_\perp^2 \rangle / 2d_{(\mathrm{zr}-o)}^2 \qquad (10)$$

where the oxygen anisotropic displacement parameter defined as $B_\perp = 8\,\pi^2 \langle u_\perp^2 \rangle$. Fig. 20 compares this to the fractional decrease in the lattice constant, illustrating that both quantities show that same temperature dependence.

This evidence is only circumstantial, but more information is available from the detailed shape of the

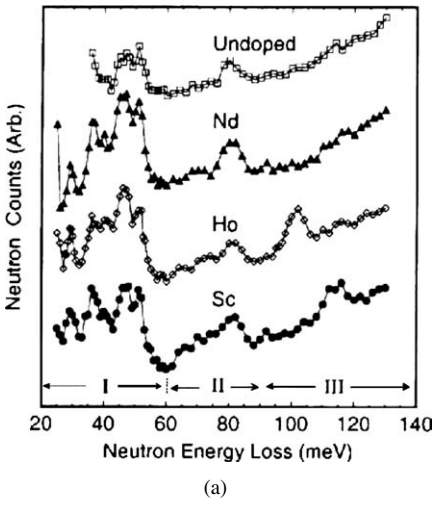

(a)

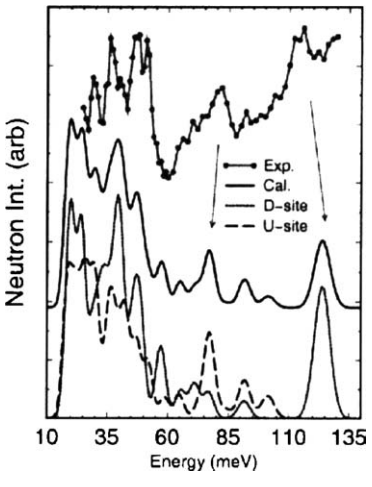

(b)

Figure 19 (a) shows the INS spectra for $ScCe_{0.95}M_xH_yO_{3+\delta}$ samples. The bending mode can be seen at 115 meV in the Sc doped sample, 105 meV in the Ho and is superimposed on the mode at 80 meV in the Nd [108]. (b) shows the results of the cluster calculations. The top curve is the experimental data on the $ScCe_{0.95}Sc_{0.05}H_xO_3$ the middle line is the calculated data. The results for the doped (D site) and undoped (U site) are shown at the bottom.

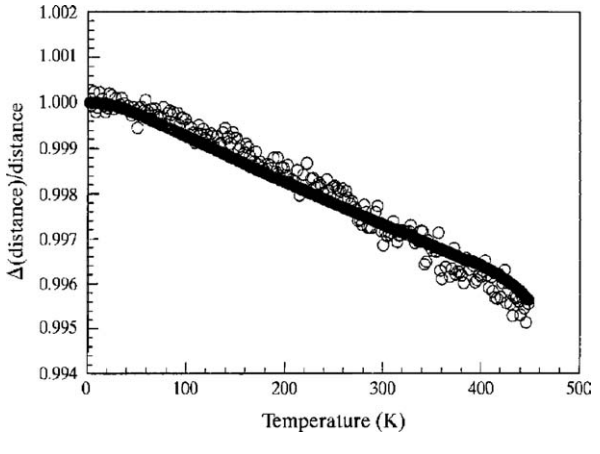

Figure 20 The data points are the fractional decrease in the lattice constant line effective Zr—O bond shortening due to correlated librational motion [113].

lattice parameter as a function of temperature. In the Gruneisen approximation there is a linear relationship between isothermal compressibility K, the coefficient of thermal expansion α and the specific heat at constant

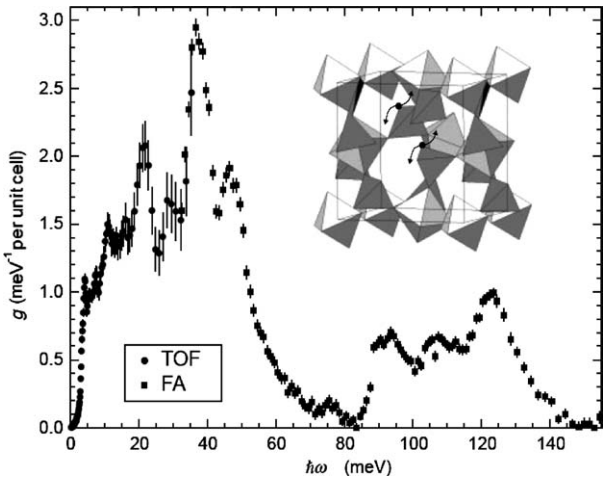

Figure 21 The generalised density of states of ZrW_2O_8 at $t = 300$ K [114].

volume C_v of the form

$$\alpha = \frac{\gamma C_v K}{V} \tag{11}$$

where the Gruneisen parameter γ is typically of the order 1-2. Integrating this gives an expression between the molar volume and the internal energy $U(T)$

$$V(T) - V(T=0) \cong \gamma K \int_0^T C_v \mathrm{d}T$$
$$= \gamma K U(T) \tag{12}$$

By using a simple model of the dynamics containing Debye and Einstein terms David *et al.* [112] were able to show that the negative thermal expansion was related to vibrational modes around 4.7 meV (55 K).

This is consistent with inelastic neutron scattering measurements [114] of the neutron weighted density-of-states (Fig. 21). By using this data to model the lattice parameter Ernst *et al.* were able to show that the Gruneisen parameter must be negative between 1.5 and 8.5 meV.

The Gruneisen parameter defines the relative change of the mode frequency with volume, $\gamma_i = -\partial \ln \omega_i / \partial \ln V$ where γ_i is the Gruneisen parameter for the ith vibrational mode. Thus the most direct way to measure the Gruneisen parameter is observe the density-of-states as a function of applied pressure. This was done by Mittal *et al.* with a 15 g sample measured at 0.3, 1.0 and 1.7 kbar [115]. From the shifts in the position of the vibrational modes it was possible to directly confirm the origin of the negative thermal expansion as due to the low energy rigid unit mode vibrations.

5.2. Piezo-electric materials

The complex perovskite ferroelectrics such as: $Pb(Zr_xTi_{1-x})O_3$ (PZT), $Pb(Zn_{1/3}Nb_{2/3})_xTi_{1-x}O_3$ (PZN) or $Pb(Mg_{1/3}Nb_{2/3})_xTi_{1-x}O_3$ (PMN) have been extensively studied, partly because of their fascinating physical properties, in particular their large piezoelectric and dielectric responses [116], but also

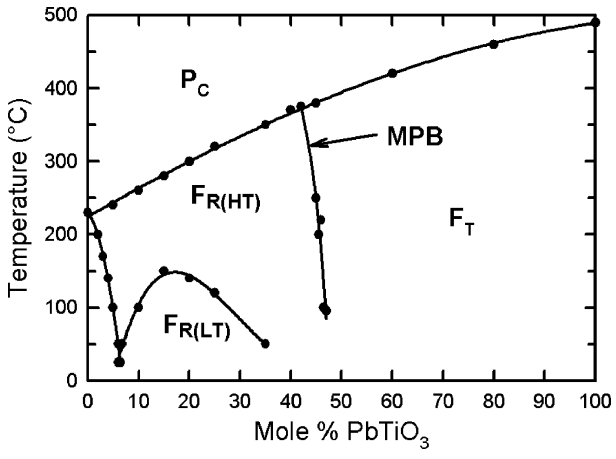

Figure 22 The phase diagram of lead zirconate titanate (PZT). Jaffe *et al.* [116].

because these properties give them immense potential for technological application. PZT ceramics are now the standard for virtually all piezoelectric sensors and actuators, but the discovery that single crystals of PZN and PZM can have piezoelectric responses 10 times that of polycrystalline PZT, is likely to lead to a revolution in electromechanical transduction for a broad range of applications. Inevitably this has also led to a frenzy of research activity in recent years.

5.2.1. The structure

X-ray diffraction has two major problems with materials such as these lead containing ceramics: Firstly the penetration depth is very low; and secondly is difficult to get accurate oxygen positions in presence of lead making it very easy to miss subtle phase changes.

The first unambiguous crystal structure of the parent compound $PbTiO_3$ was established to be tetragonal by Shirane *et al.* [117]. The doping needed to produce effective piezoelectric properties and the structural nature of the ferroelectric cubic to rhombohedral phase change was first solved by Glazer *et al*. [118, 119]. All of these studies were done with neutron scattering because of the difficulty of observing the deformations and rotations of the oxygen polyhedra as well as the displacements of the cations.

The parent compounds of the relaxor ferroelectrics ($Zn_{1/3}Nb_{2/3}O_3$ and $PbMg_{1/3}Nb_{2/3}O_3$) differ from $PbTiO_3$, in that the well defined transition between the para and ferroelectric phases is suppressed by the chemical disorder. It is replaced by a diffuse transition; characterised by a broad, frequency-dependent peak in the dielectric permittivity, but without any spontaneous polarisation appearing; indeed they remain cubic down to 5 K. The materials only develop long range ferroelectric domains if they are doped with Ti^{4+}, field cooled or subjected to high fields.

Studies of refractive index on PLZT, PMN and PZN showed that a randomly orientated local polarization develops at a well defined temperature T_d which has become known as the Burns temperature after the influential paper by Burns and Dacol [120], which is several hundred degrees above the apparent transition temperature. Around T_d these locally polarised regions are several unit-cells in size and have been called "polar nanoregions" or PNR (previously known as "polar microregions"—presumably changed for funding purposes). T_d is typically several hundred degrees, well above the diffuse transition.

For many materials a micron into the material is effectively the same as in the bulk. However, this turns out not to be the case in these ferroelectric. In an otherwise excellent measurement looking at the electric field induced phase transitions in a single crystal of PZN, Durbin *et al.* [121] used Cu $K_{\alpha 1}$ X-rays to look at the structure as a function of applied field, and saw a dramatic jump in the *c*-axis lattice parameter at around 12.5 kV/cm. Later neutron [122] and high energy synchrotron X-ray measurements [124] showed that this effect did not occur in the bulk of the sample and was in fact a "skin effect".

The piezoelectric properties of these materials are known to be at a maximum at the phase boundary between the tetragonal and rhombohedral phases, which has become known as the morphotronic phase boundary (MPB). Despite a large number of previous X-ray diffraction measurements, it was only when Noheda *et al.* [123] employed high energy synchrotron X-rays to study the structure of PZT that it was noticed that close to the boundary between the rhombohedral and tetragonal phases ($x = 0.08$) the structure could be indexed as monoclinic. This work was quickly followed by other studies that saw a similar transitional phases in both PZN [124] and PMN [125] leading to the realization that there is a universal phase diagram for the ABO_3 perovskite ferroelectric ceramics [126]. All these studies used high energy synchrotron X-rays, which, although it overcome the problems due to "skin effects", still has difficulties accurately locating the oxygen positions. In a later neutron diffraction measurement Ranjan *et al*. [127] were able to identify a new low-temperature phase below 210 K where the monoclinic cell doubles due to anti-phase rotations of neighbouring oxygen octahedra. The satellite peaks associated with this phase transition are almost invisible with X-rays.

Apart from the Bragg scattering, the relaxor ferroelectrics also show strong diffuse scattering which starts to increase in intensity below the Burns temperature [128]. From X-ray scattering studies on PMN, You and Zhang [129] concluded that the diffuse scattering was dominated by contributions from a soft transverse acoustic mode. However, the structure factors calculated from the diffuse neutron diffraction measurements [130], and the structure factor of the lowest energy TO mode from inelastic neutron scattering measurements [132] are different leading Nabrezhnov *et al.* [132] to conclude that this TO mode could not related to the ferroelectric properties of the material. This result was contradicted soon after when Gehring *et al*. [135] were finally able to observed this TO mode going soft. A potential solution to this conflict has been suggested by Hirota *et al.* [128] who pointed out that if the atoms in the PNR are uniformly shifted along their polar direction as well as being shifted due to the centre-of-mass motions of a TO mode, then the structure factors of the

X-ray and neutron diffraction and the inelastic neutron scattering can be reconciled. This uniform shift of all the atoms in the PNR with respect to surrounding (unpolarised) cubic matrix has been called a "phase shifted condensed soft mode".

5.2.2. The dynamics

To understand the microscopic origins of the ferroelectric transitions in these materials it is necessary to understand their microscopic dynamics. In a seminal experiment in the 1970's, Shirane *et al.* observed the zone centre softening of a transverse optic mode (TO) in $PbTiO_3$ using inelastic neutron scattering. The mode condenses at 490°C forcing a transition from the high temperature cubic paraelectric phase to the rhombohedral ferroelectric phase [131]. The zone centre mode energy was found to be inversely proportional to the dielectric permittivity.

$$(\hbar\omega_0)^2 = K(1/\varepsilon) = A_f(T - T_0) \qquad (13)$$

where T_0 was found to be within a few degrees of the Curie temperature.

With the discovery of the relaxor ferroelectrics such as PZN and PMN, several groups began to perform inelastic neutron scattering measurements to see if soft modes drove the behaviour in these materials.

Although the initial measurements in PMN failed to observe a soft mode, it was quickly apparent that the polar nano-regions have a significant impact on the lattice dynamics [132]. Later measurements on PMN [133] and PZN [134] as well as a crystal of PMN doped with 8% PT to bring it close to the MPB [135], all show dramatic broadening of a TO mode at momentum transfers of around 0.2 Å^{-1} (Fig. 23) below the Burns

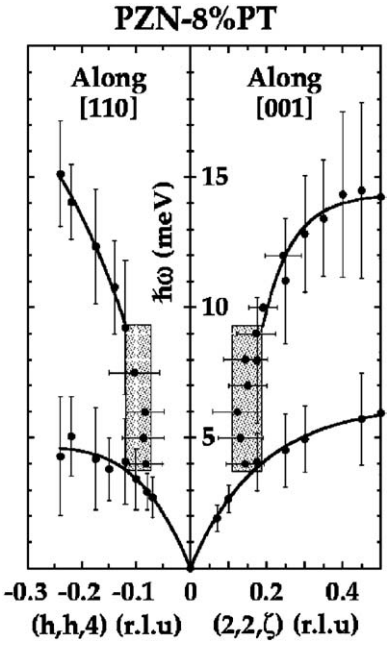

Figure 23 Data taken from inelastic neutron scattering measurement of phonon dispersion curves in PZN-8% PT (Gehring *et al.* [135]). The data was taken 500 K, which is 200 K below the Burns temperature. The bars represent the FWHM of the modes in $\hbar\omega$ and q. The TO mode broadens dramatically below $q \sim 0.2$ Å^{-1}.

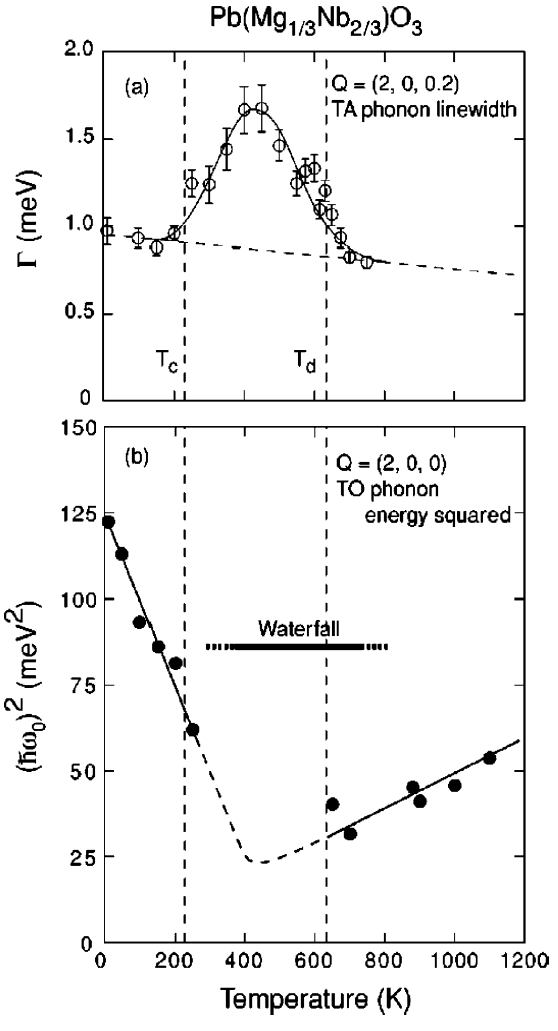

Figure 24 Inelastic neutron scattering data taken from Wakimoto *et al.* [137]. (a) The TA-phonon linewidth Γ at (2, 0, 0.2). (b) The temperature dependence of the zone centre TO mode energy squared. The vertical dashed lines correspond to $T_c = 213$ K and $T_d = 620$ K. The temperature over which the width of the TO mode is larger than its energy is shown by the solid bar.

temperature. After further measurements at different temperatures and compositions it has become widely, but not universally, accepted that this was in-fact the elusive soft-mode in the relaxor ferroelectrics [136]. The value of 0.2 Å^{-1} gives a real space dimension of several tens of Angstroms, which is constant with the work of Burns and Dacol.

Interestingly, the TO mode recovers at temperatures very close those where a field-cooled crystal will develop macroscopic ferroelectric domains. Plotting the square of the TO mode energy as a function of temperature it is possible to infer a transition temperature of 400 K (Fig. 24) in PMN [137]. The linear relationship between $(\hbar\omega_0)^2$ and $1/\varepsilon(T)$ implies that this minimum should occur at the diffuse transition temperature, $T_{max} = 265$ K, where the peak in the dielectric permittivity occurs. However, it should be remembered that this transition is strongly dependent on frequency and the lattice modes probe the dynamical response in the THz region; typical dielectric measurements are made in the KHz to MHz region.

There still remains the question of why a sharp structural transition is not seen in the relaxor ferroelectrics

despite the existence of the soft mode. A possible answer may be that the scale of the rhombohedral domains appear long range for an inelastic neutron measurement, but appear as short-range order to X-rays. In fact ferroelectric domains several tens of Angstroms in size have been report by Mathan *et al.* [138].

6. Summary

Over the last sixty years neutron scattering has changed dramatically. The first diffractometer developed by Wollan and Shull had only a single detector and took many hours or even days to make a measurement even on large samples. Despite these limitations this equipment played an important role in many of the important discoveries in condensed matter physics over the last six decades.

Today's neutron instruments have thousands of detectors and take can make measurements on samples of a fraction of a gram in a matter of seconds. This has dramatically changed the kind of science that is possible. Today studies of samples that are intrinsically small such as thin films or bio-polymers or samples in extreme environments are commonplace. The focus of interest has switch to the intrinsically weaker signals from complex or 'real world' systems.

Neutron sources are still being built with a new high-flux reactor in Munich and a replacement reactor due for completion in 2005 at Lucas Heights in Australia. Two new powerful spallation sources are also in construction a 1.4 MW source at Oak Ridge in the USA and a 1MW spallation source at JEARI in Japan, due for completion in 2006 and 2006/07. These sources are almost an order of magnitude more powerful than the best pulsed source available today and coupled with dedicated instrumentation will continue to keep neutron scattering relevant to an ever increasing range of scientific problems.

References

1. G. L. SQUIRES, "Introduction to the theory of thermal neutron scattering," Dover Publications Inc.
2. S. W. LOVESEY, "Theory of Neutron Scattering from Condensed Matter" (Oxford University Press) Vol. 1/2
3. V. F. SEARS, *Neutron News* **3** (1992) 26.
4. J. M. BESSON and R. J. NELMES, *Physica* B **213** (1995) 31.
5. http://www.ill.fr
6. http://isis.rl.ac.uk
7. C. G. SHULL, *Rev. Mod. Phys.* **67** (1995) 753.
8. E. O. WOLLAN and C. G. SHULL, *Phys. Rev.* **73** (1948) 830.
9. C. G. SHULL and E. O. WOLLAN, *ibid.* **81** (1951) 527.
10. E. O. WOLLAN, W. L. DAVIDSON and C. G. SHULL, *ibid.* **75** (1949) 1348.
11. C. G. SHULL, E. O. WOLLAN, G. A. MORTON and W. L. DAVIDSON, *ibid.* **73** (1948) 842.
12. C. G. SHULL and J. S. SMART, *ibid.* **76** (1949) 1256.
13. C. G. SHULL, *ibid.* **81** (1951) 626.
14. C. G. SHULL, E. O. WOLLAN and W. A. STRAUSER, *ibid.* **81** (1951) 483.
15. http://whisky.ill.fr/YellowBook/D20/
16. P. G. RADAELLI, A. C. HANNON and L. C. CHAPON, *Notiziario Neuroni e Luce di Sincrotrone* **8** (2003) 19.
17. W. I. F. DAVID, K. SHANKLAND, L. B. MCCLUSKER and CH. BAERLOCHER, "Structure Determination from Powder Diffraction Data" (Oxford, 2002).
18. A. K. CHEETHAM, Ab Initio Structure Solution with Powder Diffraction Data, in "The Rietveld Method," edited by R. A. Young (Oxford University Press, 1993) Chap 15, p. 276.
19. R. M. HAZEN, L. W. FINGER, R. J. ANGEL, C. T. PREWITT, N. L. ROSS, H. K. MAO, C. G. HADIDIACOS, P. H. HOR, R. L. MENG and C. W. CHU, *Phys. Rev.* B **35** (1987) 7238.
20. W. I. F. DAVID, W. T. A. HARRISON, J. M. F. GUNN, O. MOZE, A. K. SOPER, P. DAY, J. D. JORGENSEN, D. G. HINKS, M. A. BENO, L. SODERHOLM, D. W. CAPONE II, II. K SCHULLER, C. U. SEGRE, K. ZHANG and J. D. GRACE, *Nature* **327** (1897) 310.
21. A. C. LARSON and R. B. VAN DREELE, General Structural Analysis System (GSAS), Los Alamos National Laboratory Report LAUR 86-748 (2000).
22. A. WILLIAMS, G. H. KWEI, R. B. VAN DREELE, I. D. RAISTRICK and D. L. BISH, *Phys. Rev.* B **37** (1988) 7960.
23. H. IWAHARA, *Solid State Ioni*. **28–30** (1988) 573.
24. K. D. KREUER, *Annu. Rev. Mater. Res.* **33** (2003) 333.
25. K. S. KNIGHT, *Solid State Ioni.* **145** (2001) 275.
26. K. S. Knight and N. Bonanos, *J. Mater. Chem.* **4** (1994) 899.
27. W. MÜNCH, K. D. KREUER, ST. ADAMS, G. SEIFERT and J. MAIER, *Phase Transitions,* **68** (1999) 567.
28. K. D. KREUER, *Solid State Ioni.* **125** (1999) 285.
29. K. S. KNIGHT, *ibid.* **126** (2000) 43.
30. W. MÜNCH, G. SEIFERT, K.D. KREUER and J. MAIER, *ibid.* **86–88** (1996) 647.
31. W. MÜNCH, G. SEIFERT, K. D. KREUER and J. MAIER, *ibid.* **97** (1997) 39.
32. K. S. KNIGHT and N. BONANOS, *ibid.* **77** (1995) 189.
33. K. TAKEUCHI, C.-K LOONG, J. W. RICHARDSON JR., J. GUAN, S. E. DORRIS and U. BALACHANDRAN, *ibid.* **138** (2000) 63.
34. M. T. DOVE, M. G. TUCKER and D. A. KEEN, *Eur. J. Mineral.* **14** (2002) 331.
35. L. NÉEL, *Ann. De Physique* **17** (1932) 5.
36. C. G. SHULL, W. A. STRAUSER and E. O. WOLLAN, *Phys. Rev.* **83** (1951) 333.
37. C. G. SHULL and M. K. WILKINSON, *ibid.* **97** (1955) 304.
38. E. O. WOLLAN and W. C. KOEHLER, *ibid.* **100** (1955) 545.
39. G. H. JONKER and J. H. VAN SANTEN, *Physica (Vtrecht)* **16** (1950) 337.
40. J. H. VAN SANTEN and G. H. JONKER, *ibid.* **16** (1950) 599.
41. C. W. SEARLE and S. T. WANG, *Can. J. Phys.* **47** (1969) 2023.
42. C. ZENER, *Phys. Rev.* **82** (1951) 403.
43. P. W. ANDERSEN and H. HASEGAWA, *ibid.* **100** (1955) 675.
44. P. G. DE GENNES, *Phys. Rev. Lett.* **118** (1960) 141.
45. A. J. MILLIS, P. B. LITTLEWOOD and B. I. SHRAIMAN, *ibid.* **74** (1995) 5144.
46. P. DAI, J. ZHANG, H. A. MOOK, S.-H. LIOU, P. A. DOWBEN and E. W. PLUMMER, *Phys. Rev.* B **54** (1996) R3694.
47. P. G. RADAELLI, M. MAREZIO, H. Y. HWANG, S.-W. CHEONG and B. BATLOGG, *Phys. Rev.* B **54** (1996) 8992.
48. Y. MORITOMO, A. ASAMITSU, H. KUKAHARA and Y. TOKURA, *Nature* **380** (1996) 141.
49. T. KIMURA, Y. TOMIOKA, Y. KUWAHARA, H. ASAMITSU, A. TAMURA and Y. TOKURA, *Science* **274** (1996) 1698.
50. T. G. PERRING, G. AEPPLI, T. KIMURA, Y. TOKURA and M. A. ADAMS, *Phys. Rev. Lett.* **58** (1998) R14693.
51. W. KOCKELMANN and A. KIRFEL, *Physica* B (in press)
52. W. KOCKELMANN, E. PANTOS and A. KIRFEL, "Radiation in Art and Archaeometry (2000)", edited by D. C. Creagh and D. A. Bradley (Elsevier Science, 2000).
53. W. KOCKELMANN, A. KIRFEL and E. HAHNEL, *J. Archaeol. Sci.* **28** (2001) 213.

54. S. A. T. REDFERN, *Eur. J. Mineral.* **14** (2002) 251.
55. Y. LE GODEC, M. T. DOVE, D. J. FRANCIS, S. C. KOHN, W. G. MARSHALL, A. R. PAWLEY, G. D. PRICE, S. A. T. REDFERN, N. RHODES, N. L. ROSS, P. F. SCHOFIELD, E. SCHOONEVELD, G. SYFOSSE, M. G. TUCKER and W. D. WELCH, *Min. Mag.* **65** (2001) 737.
56. C. J. HOWARD and E. H. KISI, *J. Appl. Cryst.* **32** (1999) 624.
57. E. H. KISI and C. J. HOWARD, *J. Amer. Ceram. Soc.* **81** (1998) 1682.
58. T. K. GUPTA, *J. Mater. Sci.* **12** (1977) 2421.
59. K. TSUKUMA, *Amer. Ceram. Soc. Bull.* **65** (1986) 1386.
60. E. H. KISI and C. J. HOWARD, *Neutron News* **3** (1992) 24.
61. D. SIMEONE, G. BALDINOZZI, D. GOSSET, M. DUTHEIL, A. BULOU and T. HANSEN, *Phys. Rev.* B **47** (2003) 64111.
62. F. F. LANGE, *J. Mater. Sci.* **17** (1982) 224.
63. K. T. FABER, *Adv. Ceram.* **12** (1984) 293.
64. A. V. VIRKIR and R. L. K. MATSUMOTO, *Commun. Amer. Ceram. Soc.* **69** (1986) C224.
65. M. G. CAIN and M. H. LEWIS, *Mat. Lett.* **9** (1990) 309.
66. C.-J. CHAN, F. F. LANGE and M. RUHLE, *J. Amer. Ceram. Soc.* **74** (1991) 807.
67. M. G. CAIN, S. M. BENNINGTON, M. H. LEWIS and S. HULL, *Phil. Mag.* **69** (1994) 499.
68. R. I. WALTON, R. J. FRANCIS, P. SHIV HALASYAMANI, D. O'HARE, R. I. SMITH, R. DONE and R. J. HUMPHREYS, *Rev. Sci. Inst.* **70** (1999) 3391.
69. R. I. WALTON, A. NORQUIST, R. I. SMITH and D. O'HARE, *Faraday Discuss.* **122** (2002) 331.
70. D. N. ARGYRIOU, C. J. HOWARD and R. I. SMITH, *J. Amer. Ceram. Soc.* **77** (1994) 3073.
71. C. LANDRON, A. K. SOPER, T. E. JENKINS, G. N. GREAVES, L. HENNET and J. P. COUTURES, *J. Non-Cryst. Solids* **293–295** (2001) 453.
72. S. ANSELL, J. K. KRISHNAN, J. J. FELTON, P. C. NORDINE, M. A. BENO, D. L. PRICE and M. L XABOUGI, *Phys. Rev. Lett.* **78** (1997) 464.
73. A. MANTHIRAM, 'Battery Applications', in "Encyclopedia of Smart Materials," edited by M. Schwartz (Jon Wiley & Sons, 2003).
74. M. M. THACKERAY, W. I. F. DAVID, P. G. BRUCE and J. B. GOODENOUGH, *Mater. Res. Bull.* **18** (1983) 472.
75. A. R. ARMSTRONG and P. G. BRUCE, *Nature* **381** (1996) 499.
76. E. LEVIO, M. D. LEVI, G. SALITRA, D. AURBACH, R. OESTEN, U. HEIDER and L. HEIDER, *Sol. St. Ion.* **126** (1999) 109.
77. H. BERG, H. RUNDLÖV and J. O. THOMAS, *ibid.* **144** (2001) 65.
78. A. D. ROBERTSON, A. R. ARMSTRONG, A. J. PATERSON, M. J. DUNCAN and P. G. BRUCE, *J. Mater. Chem.* **13** (2003) 2367.
79. B. N. BROCKHOUSE, *Rev. Mod. Phys.* **67** (1995) 735.
80. B. N. BROCKHOUSE and A. T. STEWERT, *Phys. Rev.* **100** (1955) 756.
81. B. N. BROCKHOUSE, *ibid.* **106** (1957) 859.
82. B. N. BROCKHOUSE, L. N. BECKA, K. R. RAO, R. N. SINCLAIR and A. D. B. WOODS, *J. Phys. Soc. Jpn.* **17** (1962) 63.
83. B. N. BROCKHOUSE, K. R. RAO and A. D. B. WOODS, *Phys. Rev. Lett.* **7** (1961) 93.
84. W. COCHRAN, *ibid.* **3** (1959) 412.
85. R. A. COWLEY, *ibid.* **9** (1962) 159.
86. P. A. FLEURY, J. F. SCOTT and J. M. WORLOCK, *ibid.* **21** (1968) 16.
87. Y. YAMADA and G. SHIRANE, *Phys. Rev.* **177** (1969) 858.
88. R. A. COWLEY, W. J. L. BUYERS and G. DOLLING, *Sol. State. Comm.* **7** (1969) 181.
89. T. G. PERRING, G. AEPPLI, S. M. HAYDEN, S. A. CARTER, J. P. REMEIKA and S.-W. CHEONG, *Phys. Rev. Let.* **77** (1996) 711.
90. N. FURUKAWA, *J. Phys. Soc. Jpn.* **65** (1996) 1174.
91. H. Y. HWANG, P. DAI, S.-W. CHEONG, G. AEPPLI, D. A. TENNANT and H. A. MOO, *Phys. Rev. Lett.* **80** (1998) 1316.
92. P. DAI, H. Y. HWANG, J. ZHANG, J. A. FERNANEEZ-BACA, S.-W. CHEONG, C. KLOC, Y. TOMIOKA and Y. TOKURA, *Phys. Rev.* B **61** (2000) 9553.
93. T. CHATTERJI, L. P. REGNAULT and W. SCHMIDT, *ibid.* **66** (2002) 214408.
94. T. G. PERRING, D. T. ADROJA, G. CHABOUSSANT, G. AEPPLI, T. KIMURA and Y. TOKURA, *Phys. Rev. Lett.* **87** (2001) 217201.
95. G. AEPPLI, D. J. BISHOP, C. BROHOLM, E. BUCHER, S.-W. CHEONG, P. DAI, Z. FISK, S. M. HAYDEN, R. KLEIMAN, T. E. MASON, H. A. MOOK, T. G. PERRING and A. SCHROEDER, *Physica* C **317/318** (1999) 9.
96. D. VAKNIN, S. K. SINHA, D. E. MONCTON, D. C. JOHNSTON, J. M. NEWSAM, C. R. SAFINYA and H. E. KING JR., *Phys. Rev. Lett.* **58** (1987) 2802.
97. S.-W. CHEONG, G. AEPPLI, T. E. MASON, H. MOOK, S. M. HAYDEN, P. C. CANFIELD, Z. FISK, K. N. CLAUSEN and J. L MARTINEZ, *ibid.* **67** (1991) 1791.
98. H. A. MOOK, P. C. DAI, S. M. HAYDEN, G. AEPPLI, T. G. PERRING and F. DOGAN, *Nature* **395** (1998) 580.
99. G. AEPPLI, *Science* **278** (1997) 1432.
100. K. YAMADA, C. H. LEE, K. KURAHASHI, J. WADA, S. WAKIMOTO, S. UEKI, H. KIMURA and Y. ENDOH, *Phys. Rev.* B **57** (1998) 6165.
101. J. P. GOFF, W. HAYES, S. HULL, M. T. HUTCHINGS and K. N. CLAUSEN, *ibid.* B **59** (1999) 14202.
102. R. HEMPELMANN, CH. KARMONIK, TH. MATZKE, M. CAPPADONIA, U. STIMMING, T. SPRINGER and M. A. ADAMS, *Sol. St. Ion.* **77** (1995) 152.
103. R. HEMPELMANN, *Physica* B **226** (1996) 72.
104. C. T. J. GROTTHAUS, *Ann. Chem.* **LVIII** (1806) 54.
105. M. S. ISLAM, R. A. DAVIES and J. D. GALE, *Chem. Mater.* **13** (2001) 2049.
106. W. MÜNCH, K. D. KREUER, G. SEIFERT and J. MAIER, *Solid State Ion.* **125** (1999) 39.
107. C. KARMONIK, T. J. UDOVIC, R. L. PAUL, K. LIND and R. HEMPELMANN, *ibid.* **109** (1998) 207.
108. T. YILDIRIM, B. REISNER, T. J. UDOVIC and D. A. NEUMANN, *ibid.* **145** (2001) 429.
109. J. S. O. EVANS, T. A. MARY, T. VOGT, M. A. SUBRAMANIAN and A. W. SLEIGHT, *Chem. Matter.* **8** (1996) 2809.
110. T. A. MARY, J. S. O. EVANS, T. VOGT and A. W. SLEIGHT, *Science* **272** (1996) 90.
111. S. M. BENNINGTON, J. C. LI, M. J. HARRIS and D. K. ROSS, *Physica* B **263** (1999) 396.
112. W. I. F. DAVID, J. S. O EVANS and A. W. SLEIGHT, Europhys. *Lett.* **46**(5) (1999) 661.
113. J. S. O. EVANS, W. I. F. DAVID and A. W. SLEIGHT, *Acta Cryst.* B **55** (1999) 333.
114. G. ERNST, C. BROHOLM, G. R. KOWACH and A. P. RAMIREZ, *Nature* **396** (1998) 147.
115. R. MITTAL, S. L. CHAPLOT, H. SCHOBER and T. A. MARY, *PRL* **86** (2001) 4692.
116. B. JAFFE, W. R. COOK and H. JAFFE, "Piezoelectric Ceramics" (Academic Press, London, 1971).
117. G. SHIRANE, R. PEPINSKY and B. C. FRAZER, *Acta Cryst.* **9** (1956) 131.
118. A. M. GLAZER and S. A. MABUD, *ibid.* B **34** 1065.
119. A. M. GLAZER, S. M. MABUD and R. CLARKE, *ibid.* B **34** (1978) 1060.
120. G. BURNS and F. H. DACOL, *Solid State Commun.* **48** (1983) 853.
121. M. K. DURBIN, E. W. JACOBS, J. C. HICKS and S.-E PARK, *Appl. Phys. Lett.* **74** (1999) 2848.
122. K. OHWADA, K. HIROTA, P. W. REHRIG, P. M. GEHRING, B. HOHEDA, Y. FUJII, S.-E. PARK and G. SHIRANE, *J. Phys. Soc. Jpn* **70** (2001) 2778.

123. B. NOHEDA, D. E. COX G. SHIRANE, J. A. GONZALO, L. E. CROSS, and S.-E. PARK, *Appl. Phys. Lett.* **74** (1999) 2059.
124. B. NOHEDA, D. E. COX, G. SHIRANE, S.-E. PARK, L. E. CROSS and Z. ZHONG, *PRL* **86** (2001) 3891.
125. Z.-G. YE, B. NOHEDA, M. DONG, D. COX and G. SHIRANE, *Phys. Rev.* B **64** (2001) 184114.
126. D. E. COX, N. NOHEDA, G. SHIRANE, Y. UESA, K. FUJISHIRO and Y. YAMADA, *Appl. Phys. Lett.* **79** (2001) 400.
127. R. RANJAN, RAGINI, S. K. MISHRA, D. PANDEY and B. J. KENNEDY, *Phys. Rev.* **65** (2002) 60102.
128. K. HIROTA, Z.-G. YE, S. WAKIMOTO, P. M. GEHRING and G. SHIRANE, *ibid.* B **65** (2002) 104105.
129. H. YOU and Q. M. ZHANG, *Phys. Rev. Lett.* **79** (1997) 3950.
130. S. B. VAKHRUSHEV, A. A. NABEREZNOV, N. M. OKUEVA and B. N. SAVENKO, *Phys. Solid State* **37** (1995) 1993.
131. G. SHIRANE, J. D. AXE, HARADA and J. P. REMEIKA, *Phys. Rev.* B **2** (1970) 155.
132. A. NABEREZHNOV, S. VAKHRUSHEV, B. DORNER, D. STRAUCH and H. MOUDDEN, *Eur. Phys. J.* B **11** (1999) 13.
133. P. M GEHRING, S. WAKIMOTO, Z.-G YE and G. SHIRANE, *Phys. Rev. Lett.* **87** (2001) 277601.
134. P. M. GEHRING, S.-E. PARK and G. SHIRANE, *Phys. Rev.* B **63** (2001) 224109.
135. P. M. GEHRING, S.-E. PARK and G. SHIRANE, *Phys. Rev. Lett.* **84** (2000) 5216.
136. P. M. GEHRING, S. WAKIMOTO, Z.-G. YE and G. SHIRANE, *ibid.* **87** (2001) 277601.
137. S. WAKIMOTO, C. STOCK, R. J. BIRGENEAU, Z.-G. YE, W. CHEN, W. J. L. BUYERS, P. M. GEHRING and G. SHIRANE, *Phys. Rev.* B **65** (2002) 172105.
138. N. DE MATHAN, E. HUSSON, G. CALVARIN, J. R. GAVARRI, A. W. HUWAT and A. MORELL, *J. Phys. Condens. Matter* **3** (1991) 8159.

Received 10 December 2003
and accepted 20 January 2004